Accepted Manuscript

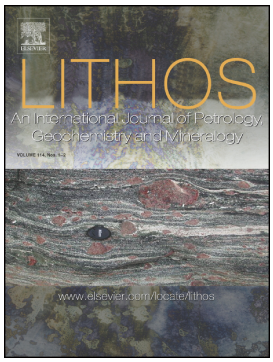

Mesozoic high-Mg andesites from the Daohugou area, Inner Mongolia: Upper-crustal fractional crystallization of parental melt derived from metasomatized lithospheric mantle wedge

Fanxue Meng, Shan Gao, Zhaojun Song, Yaoling Niu, Xuping Li

PII: S0024-4937(18)30042-2
DOI: https://doi.org/10.1016/j.lithos.2018.01.032
Reference: LITHOS 4559

To appear in:

Received date: 24 July 2017
Accepted date: 23 January 2018

Please cite this article as: Fanxue Meng, Shan Gao, Zhaojun Song, Yaoling Niu, Xuping Li , Mesozoic high-Mg andesites from the Daohugou area, Inner Mongolia: Upper-crustal fractional crystallization of parental melt derived from metasomatized lithospheric mantle wedge. The address for the corresponding author was captured as affiliation for all authors. Please check if appropriate. Lithos(2018), https://doi.org/10.1016/j.lithos.2018.01.032

Mesozoic high-Mg andesites from the Daohugou area, Inner Mongolia: upper-crustal fractional crystallization of parental melt derived from metasomatized lithospheric mantle wedge

Fanxue Meng [a,b,*], Shan Gao [c], Zhaojun Song [a,*], Yaoling Niu [d,e]

Xuping Li [a]

[a] College of Earth Science and Engineering, Shandong University of Science and Technology, Qingdao 266590, China

[b] Laboratory for Marine Geology, Qingdao National Laboratory for Marine Science and Technology, Qingdao 266061, China

[c] State Key Laboratory of Geological Processes and Mineral Resources, China University of Geosciences, Wuhan 430074, China

[d] *Institute of Oceanology, Chinese Academy of Sciences, Qingdao 266071, China*

[e] Department of Earth Sciences, Durham University, DH1 3LE, UK

* Corresponding author. Tel.: +86 13665327810.

E-mail address: mfx1117@163.com

Jan. 11, 2018 version

Abstract

Mineral chemistry, major- and trace-element data, zircon U–Pb ages, and Sr–Nd isotopic data are presented for a suite of volcanic rocks from the Daohugou area, Ningcheng City, Inner Mongolia, on the northern margin of the North China Craton. Samples from the suite are of basaltic andesite to rhyolite in composition, with the rocks containing <60 wt. % SiO_2 have high MgO, Cr, and Ni contents, and classify as high-Mg andesites (HMAs). Zircons from a rhyolite yielded weighted mean $^{206}Pb/^{238}U$ age of 164±1 Ma, indicating that the Daohugou volcanic suite is coeval with the Tiaojishan Formation of northern Hebei and western Liaoning Province. The HMAs have similar enriched-mantle I (EMI)-type isotopic compositions to each other, with low $\varepsilon_{Nd}(t)$ values, moderate $(^{87}Sr/^{86}Sr)_i$ ratios, enrichment in LREEs relative to LILEs, and depletion in HFSEs (e.g., Nb, Ta, Ti), indicating formation through protracted fractional crystallization of a common parental magma. The unusually low CaO contents and CaO/FeO ratios of olivine phenocrysts in the HMAs suggest that the parental melt was subduction-related. The results of Rhyolite-MELTS modelling indicates that HMAs may form through upper-crustal fractional crystallization from arc basalts. Therefore, the Daohugou HMAs were most likely formed through fractional crystallization of a parental melt derived from metasomatized lithospheric mantle at crustal depths. The addition of "water" to the cratonic keel may have played a key role in the destruction of the North China Craton.

Key words: High-Mg andesite; North China Craton; Metasomatized lithospheric mantle; Upper crustal fractional crystallization.

1. Introduction

The ancient, cratonic mantle lithosphere, similar to that beneath the Kaapvaal, Siberian, and other Archean cratons, was removed from the base of the Eastern Block of the North China Craton (NCC) during the Mesozoic, and partly replenished with younger, less refractory lithospheric mantle (Menzies et al., 1993; Griffin et al., 1998; Menzies and Xu, 1998; Zheng, 1999; Fan et al., 2000; O'Relly et al., 2001; Xu, 2001; Zheng et al., 2001, 2007; Gao et al., 2002, 2004; Zhang et al., 2003; Xu Y G et al., 2008). As a consequence, the composition, thermal structure, and thickness of the sub-continental lithospheric mantle (SCLM) of the North China Craton changed dramatically, although the mechanisms and timing of the changes are debated (Niu, 2005). The widespread Mesozoic volcanic rocks in eastern China, especially basalts and high-Mg andesites (HMAs), provide a window into mantle sources and processes, including the evolution of the lithospheric mantle beneath the NCC.

The term "high-Mg andesite" was first used in reference to a suite of andesitic volcanic rocks from Adak Island in the Aleutians (Kay, 1978). HMAs have elevated Mg numbers ($Mg^{\#}$=100× Mg/(Mg + Fe^{2+})), high abundances of large-ion lithophile elements (LILEs), high Sr/Y ratios, and were previously thought to be derived from partial melting of subducted oceanic crust where the melt interacted with mantle peridotite during ascent (e.g., Kay, 1978; Defant and Drummond, 1990; Liu et al., 2012; Sato et al., 2014). HMAs can, however, be generated by other processes in a range of tectonic settings (e.g., Castillo, 2012), including melting of a metasomatized

mantle peridotite (Shirey and Hanson, 1984; Kelemen, 1995; Hirose, 1997; Calmus et al., 2003), and partial melting of delaminated lower continental crust, with the melts rising and interacting with mantle peridotite (Kay and Kay, 1993; Xu et al., 2002; Chung et al., 2003; Gao et al., 2004; Huang et al., 2008; Rapp et al., 2010). In all three of the above models, the initial partial melting of the mafic crust and/or assimilation of ultramafic rocks occur at mantle depths. However, some HMAs are considered to be derived from crustal-level magma mixing or fractional crystallization (Streck et al., 2007; Qian and Hermann, 2010; Shellnutt and Zellmer, 2010; Chen et al., 2014). The pressure of HMA formation is therefore important, and can be estimated from the H_2O content of melt inclusions. Previous experimental work on HMAs has shown that when these rocks are generated by partial melting of wet peridotite in the upper mantle, their minimum water contents are on the order of ~10 wt. % (Grove et al., 2005). Shellnutt and Zellmer (2010) demonstrated that HMAs (which have been regarded as particularly hydrous primary melts generated in equilibrium with mantle peridotite) can form by fractional crystallization from low-H_2O primitive arc basalts in the upper crust. Humphreys et al. (2006) reported that the crystallization of some Shiveluch HMAs took place within the upper crust. A recent study of HMAs from Xinkailing in Western Liaoning, China, provided an opportunity to investigate the origin and evolution of subduction-modified lithospheric mantle at the northern margin of the North China craton (Hong et al., 2017), and suggested a hydrous (2–6 wt. % H_2O) orthopyroxene-rich pyroxenite source.

Here, mineral chemistry, zircon U–Pb ages, major- and trace-element data, and Sr–Nd isotopic compositions are presented for the Daohugou volcanic rocks, with the aim of improving our understanding of the petrogenesis of the Daohugou HMAs and the geological evolution of eastern China during the Mesozoic.

2. Geological setting and sample description

The North China Craton is one of the world's oldest Archean cratons, preserving crustal remnants as old as 3800 Ma (Liu et al., 1992, 2008; Song et al., 1996). It is surrounded by the Mesozoic Dabie and Sulu orogenic belts to the south and east (Li et al., 1993; Meng and Zhang, 2000), and by the Central Asian Orogenic Belt to the north (Sengör et al., 1999). The craton is divided into the Eastern and Western Blocks by the Trans-North China Orogen/Central Orogenic Belt (Zhao et al., 2005; Santosh, 2010; Zhai and Santosh, 2011; Zhao and Zhai, 2013) (Fig. 1).

Ningcheng City, in Inner Mongolia, is located at the northern margin of the NCC, within the central part of the Yanshanian orogenic belt. The Ningcheng basin basement comprises predominantly Archean and Mesoproterozoic rocks that are unconformably overlain by late Mesozoic Jurassic–Cretaceous volcanic sedimentary rocks (Fig. 1). These well studied late Mesozoic volcano-sedimentary sequences comprise, from the stratigraphic base upwards, the Jiulongshan Formation, Tiaojishan Formation, and Lower Cretaceous Tuchengzi and Yixian Formations (Liu et al., 2006). The Tuchengzi Formation in western Liaoning is considered to be Late Jurassic (J3tc) in age (Hong et al., 2017).

Samples were collected from the Daohugou area of Ningcheng City, ~ 80 km

south of Chifeng City, Inner Mongolia (Wang et al., 2006), and ~ 30 km north of Lingyuan City, Liaoning Province, China (Ji et al., 2002). Previous studies focused mainly on the geochronology of Daohugou strata because of their abundant fauna and flora fossils. $^{40}Ar/^{39}Ar$ dating of an ignimbrite yielded an age of 159.8 ± 0.8 Ma (He et al., 2004). Sensitive high-resolution ion microprobe (SHRIMP) zircon U–Pb analyses and plagioclase $^{40}Ar–^{39}Ar$ dating of intermediate to felsic rocks overlying the Daohugou fossiliferous sediments gave ages of 164–165Ma (Chen et al., 2004). U–Pb dating of the Daohugou lavas (Liu et al., 2006) gave similar ages of 165–152Ma. SHRIMP U–Pb dating of zircons collected from a tuff layer and an andesite flow yielded ages of 165.0 ± 1.2 Ma and 164.3 ± 2.2 Ma, respectively (Yang and Li, 2008). Together, these data suggest that the Daohugou strata is coeval with the Tiaojishan/Lanqi Formation in northern Hebei and western Liaoning.

Samples were collected from the Jiangzhangji section (N 41°25′, E 119°16′), comprising basaltic trachyandesite and overlying rhyolite. The HMAs are greyish-green and porphyritic, containing clinopyroxene and olivine. Plagioclase is the only phenocryst phase in the dacite and rhyolite (Appendix Fig. A1).

3. Analytical methods

3.1 Mineral analyses

The major element compositions of minerals were measured at the State Key Laboratory of Geological Processes and Mineral Resources, China University of Geosciences in Wuhan, China, with a JEOL JXA–8100 Electron Microprobe Analyzer equipped with four wavelength-dispersive spectrometers (WDS). The

polished thin-sections were firstly coated with a thin conductive carbon film prior to analysis. The precautions suggested by Zhang and Yang (2016) were used to minimize the difference of carbon film thickness between samples and obtain a ca. 20 nm approximately uniform coating. An accelerating voltage of 20 kV, a beam current of 20 nA, and a 2 μm spot diameter were used to analyze minerals. Data were corrected on-line using a modified ZAF (atomic number, absorption, fluorescence) correction procedure. The peak counting time was 10 s for Na, Mg, Al, Si, K, Ca, Fe and 20 s for Ti and Mn. The background counting time was one-half of the peak counting time on the high- and low-energy background positions. Silicates and pure oxides (Sanidine (K), Pyrope Garnet (Fe, Al), Diopsode (Ca, Mg), Jadeite (Na), Rhodonite (Mn), Olivine (Si), Rutile (Ti)) were used as standards for calibration.

3.2 Zircon U-Pb dating

Zircons were separated from samples by traditional heavy–liquid and magnetic methods and then purified by hand picking under a binocular microscope. Zircon grains were selected and mounted on a double-sided tape, cast in epoxy resin, and polished to expose surfaces suitable for U–Pb dating.

The Cathodoluminescence (CL) images were used to show the internal textures of zircons and to select optimum spots for U–Pb dating. The CL images of zircons were obtained using Carlzeiss Merlin Compact high resolution scanning electron microscope connected with an Oxford IE250 energy dispersive system and a Gatan Mono CL4 CL system in the Beijing SHRIMP Center, Chinese Academy of Geological Sciences (CAGS), China.

Zircons were dated using the SHRIMP II ion microprobe at the Beijing SHRIMP Center, CAGS, China. Analytical procedures and conditions were similar to those described by Williams (1998). Mass resolution during the analytical sessions was ~5000 (1% peak height on the UO-peak of the standard). The intensity of the primary O^{-2} ion beam was 3–4 nA. Spot size was ~30 μm in diameter, and each site was rastered for 180 s prior to analysis to remove surface contamination. Reference zircons M257 (U = 840 ppm, Nasdala et al., 2008) and TEMORA 1 ($^{206}Pb/^{238}U$ age = 417 Ma, Black et al., 2003) were used to calibrate the U abundance and U–Pb age, respectively. TEMORA 1 was analyzed once every 3–4 unknown analyses. Mass analysis at each spot consisted of five scans through the mass stations. Common lead correction was applied using the measured ^{204}Pb abundances. Data processing was carried out using the SQUID and ISOPLOT programs (Ludwig, 2001, 2003). Uncertainties of individual analyses are reported at 1σ; mean weighted $^{207}Pb/^{206}Pb$ ages were calculated at 95% confidence.

3.3 Major and trace element analysis

Rock samples were trimmed to remove altered surfaces and crushed to a grain size of <200 mesh for major and trace element, and isotopic analyses. Major elements were analyzed using an X–ray fluorescence (XRF; Rikagu RIX 2100) on fused glass disks at Northwest University, China, following Rudnick et al. (2004).

For trace element analyses, samples were digested using a mixture of HF + HNO_3 in Teflon bombs and analyzed with an Agilent 7500a ICP-MS at Northwest University, China following Rudnick et al. (2004). Results of the USGS rock

standards (BHVO–1, BCR–2 and AGV–1) indicate accuracies and precisions better than 5% for all elements except for Ni, Ta and Th, which are 5%–10%. The analytical results of these standards are given in Table S2.

3.4 Sr-Nd isotope analysis

Sr, Nd isotopic compositions were determined using MC–ICP–MS (Nu Plasma HR, Nu Instruments, Wrexham, UK) in static mode at Northwest University, China.

For Sr–Nd isotopes, ~ 100 mg rock power was digested in a sealed Teflon bomb with a mixture of concentrated HNO_3, HF and $HClO_4$. The sealed bombs were kept in an oven at 190°C for 48 hours. The decomposed samples were then dried at 140°C followed by adding concentrated HNO_3 and HCl. Sr and Nd (and other REEs) were separated/concentrated using standard chromatographic columns with AG50W–X8 and HDEHP resins following Gao et al. (2004). The measured $^{143}Nd/^{144}Nd$ and $^{87}Sr/^{86}Sr$ ratios were normalized to $^{146}Nd/^{144}Nd = 0.7219$ and $^{86}Sr/^{88}Sr = 0.1194$, respectively. External reproducibility of the isotopic measurement was monitored by repeated analysis of international standards. Repeated analyses of La Jolla along with unknown samples gave an average $^{143}Nd/^{144}Nd$ of 0.511835±0.000001 (2σ, n=13), and NBS 987 gave $^{87}Sr/^{86}Sr$ =0.710191±0.000002 (2σ, n=12), which is identical to reference values within analytical error. Analysis of BCR–2 gave $^{87}Sr/^{86}Sr$=0.705003± 0.00001 (2σ), $^{143}Nd/^{144}Nd$=0.512622±0.000001 (2σ). Procedural blanks are about<20pg and <40pg for Nd and Sr, respectively.

4. Analytical data

4.1 Mineral chemistry

4.1.1 Olivine

HMA olivine compositions are listed in Table A1. Olivine crystals have Fo (Fo = 100×Mg/(Mg + Fe)) values of 78–83, and relatively narrow ranges of CaO contents and CaO/FeO ratios, similar to those within the Xinkailing HMAs of western Liaoning (Fig. 2). They generally exhibit low CaO contents and CaO/FeO ratios. In olivine compositional diagrams (Fig. 2), they plot within the field of subduction-related lavas, and outside the field of non-subduction-related lavas (including mid-ocean-ridge and ocean-island basalts; MORB and OIB) (Fig. 2).

4.1.2 Clinopyroxene

Clinopyroxene phenocrysts in the HMAs are mostly augite ($En_{41-45}Fs_{12-15}Wo_{43-44}$), with some exhibiting the reverse compositional zoning with high-Fe and low-Mg in the core and high-Mg in the rim (Table S1; Fig. A2). Reverse compositional zoning has also been reported in orthopyroxene phenocrysts in Xinglonggou HMAs from western Liaoning (Gao et al., 2004).

4.2 Geochronology

Seventeen zircon grains from one rhyolite sample located at the upper unit of the Daohugou sequence (sample DHG-57) were dated using SHRIMP II ion microprobe. U-Pb zircon data are summarized in Table S3. The zircons are typically euhedral to subhedral, have Th/U ratios of > 0.5, and are characterized by oscillatory zoning (Fig. 3) , suggesting a magmatic origin. The zircons have a weighted mean $^{206}Pb/^{238}U$ age of 164 ± 1Ma (MSWD=0.27, n=17) (Fig. 4).

4.3 Major and Trace elements

Representative major- and trace-element data are given in Table 1, with full data provided in Supplementary Table S4. In the total alkalis vs. silica (TAS) diagram (Le Maitre et al., 1989), the samples plot in the alkaline field, and consist mainly of trachyandesite and trachyte with minor basaltic trachyandesite and rhyolite (Fig. 5). They have SiO_2 and MgO contents of 54.44–74.57 wt. % and 0.03–6.05 wt. %, respectively. Most samples with SiO_2 contents of < 60 wt. % have high MgO content (>3 wt. %) and Mg# values, similar to the HMAs (Gao et al., 2008). On major-element vs. SiO_2 diagrams (Fig. 6), they exhibit broad trends except for an abrupt decrease in Na_2O and Al_2O_3 contents with increasing SiO_2 content.

Chondrite-normalized REE patterns are characterized by enrichment in light rare-earth elements (LREEs) relative to heavy REEs (HREEs). Eu anomalies are insignificant (Eu/Eu* = 0.92–1.17) for all the samples except the rhyolites (Fig. 7a). In the primitive-mantle normalized trace-element diagram (Fig. 7b), the samples display a pronounced depletion in high field strength elements (HFSEs; e.g., Nb, Ta, Ti), and enrichment in large ion lithophile elements (LILEs) relative to LREEs and HFSEs. The samples exhibit positive Ba, K, and Pb anomalies. HMAs display positive Sr anomalies, and samples with SiO_2 contents above 60 wt. %, show negative Sr anomalies. This can be explained by fractional crystallization of plagioclase, as supported by the positive correlation between Sr and SiO_2 at SiO_2 contents below ~60 wt. % and negative correlation above ~60 wt. % (Fig. 8). The Sr content is 21–1489 ppm over the entire sample suite, with the HMAs having the higher concentrations (981–1489 ppm), and Sr/Y ratios are 53–112 (Table 2), similar to adakites (Defant

and Drummond, 1990; Kay and Kay, 1993; Martin et al., 2005). However, in a plot of Sr/Y vs. Y (Fig. 11), the HMAs plot in the field of typical arc rocks with higher Y contents (16.6–19.7 ppm). They also have high Cr (173–230 ppm) and Ni (73–133 ppm) contents, similar to those documented from the type locality of HMA by Kay (1978).

4.4 Sr–Nd isotopes

Sr and Nd isotope data are given in Table 2. Initial Sr and Nd isotopic compositions were calculated to the time of formation at 160 Ma using the measured Sr–Nd isotopic composition and parent/daughter ratios. The ε_{Nd} (t) are calculated using (10, 000 × [($^{143}Nd/^{144}Nd$)sample/($^{143}Nd/^{144}Nd$)chondrite-1]), in which, subscript sample and chondrite denote values of sample and chondrite at the time of sample formation, and the ($^{143}Nd/^{144}Nd$)chondrite = 0.512638 (Dickin, 1997). The samples display moderate Sr and low Nd isotopic ratios, similar to EMI-type isotope features, with $(^{87}Sr/^{86}Sr)_i$ = 0.705230–0.706402, $^{143}Nd/^{144}Nd_i$=0.511735–0.511944, and $\varepsilon_{Nd\ (t)}$ = –11.8 to –15.4 (Fig. 12).

5. Discussion

5.1 Fractional crystallization

The Daohugou samples consist of basaltic trachyandesite, trachyandesite, and rhyolite. The strong correlations displayed in the variation diagrams (Fig. 6) could be due either to varying degrees of fractional crystallization from a common parental magma, or to mixing of basaltic melts with crustal melts. The similarities between isotopic compositions and trace-element systematics of the samples do not favor a

mixing model. However, their similar isotopic compositions indicate a genetic relationship, with the felsic melts derived from protracted fractional crystallization. The Rhyolite-MELTS (Gualda and Ghiorso, 2015) was used to model Daohugou HMA evolution at varying pressures (1 and 10 kbar), water contents (4% and 0.5%) and oxygen fugacities (NNO, NNO + 1, and NNO + 2, where NNO is the nickel–nickel oxide buffer) (Figs. 9 and 10). The most primitive basaltic rocks (DHG 67) in this study was used as the starting composition (Appendix 1), The results are broadly consistent with fractional crystallization along the liquid lines of descent of olivine, spinel and clinopyroxene, and then feldspar, orthopyroxene, accessory Fe–Ti oxides and apatite at lower pressure (1kbar), ~4 wt. % H_2O content and higher oxygen fugacities (NNO + 1, and NNO + 2, (Fig. 9). The proportions of crystallized minerals at 1 kbar, with NNO+2 fugacity and 4 wt. % H_2O are listed in Appendix 1.

Trace-element variation diagrams (Fig. 8), are also consistent with the fractionation modelling. The trace-element contents of the most primitive basalt (DHG67) were used as the starting composition, with mineral/melt partition coefficients as summarized in Appendix 1. The SiO_2 content was on basis of the Rhyolite-MELTS modelling at a pressure of 1kbar, 4 wt. % H_2O, and high fO_2 (NNO+2). The fractional crystallization trend is shown in Fig. 8 and the tick marks at 20% intervals represent percentage of crystallization. The modelling results are in good agreement with the HMA compositions. The highly compatible elements, Cr and Ni, are rapidly depleted as MgO contents approach zero as a result of the removal of 8% spinel, 6% olivine, 14% clinopyroxene, 7% orthopyroxene, and 45%

plagioclase (Fig. 8). Sr contents and Sr/Y ratios increase with increasing SiO_2, reaching a maxima at SiO_2 content of ~ 60 wt. %, as a result of the fractionation of olivine, clinopyroxene, and spinel prior to the crystallization of plagioclase, because Sr is incompatible in spinel, olivine and clinopyroxene, but highly compatible in plagioclase. The observation that Nb content decreases with increasing SiO_2 content may be due to the high compatibility of Nb in Fe–Ti oxides such as ilmenite (Green and Pearson, 1987).

5.2 Petrogenesis of HMAs

Our geochemical data demonstrate that the samples with $SiO_2 < 60$ wt. % mostly have relatively high MgO (> 3 wt. %), Cr and Ni contents and are termed as HMAs. It has been suggested that HMAs reflect the interaction of the partial melt of subducted eclogite with the mantle wedge (Kay, 1978; Defant and Drummond, 1990; Kelemen et al., 2003). However, the relatively high $(^{87}Sr/^{86}Sr)_i$ ratios, negative $\varepsilon_{Nd}(t)$ values, and non-ragiogenic Pb isotopic compositions of the Daohugou HMAs do not support their derivation from subducted oceanic crust. Furthermore, the "adakitic" signatures of the Daohugou HMAs are relatively weak in terms of HREE and Y depletion (Fig. 11), indicating that little or no garnet was involved in their petrogenesis. Alternatively, the HMAs could represent primary magmas in equilibrium with mantle peridotite (Tatsumi and Ishizaka 1981; Shirey and Hanson, 1984; Kelemen, 1995; Hirose, 1997; Calmus et al., 2003) or the interaction of partial melts of delaminated lower continental crust and mantle peridotite (Kay and Kay, 1993; Xu et al., 2002; Chung et al., 2003; Gao et al., 2004; Huang et al., 2008; Rapp et al., 2010). It is also possible

that the HMAs do not represent primary magma. Fractional crystallization of basaltic magmas has previously been used to explain the petrogenesis of HMAs (e.g., Baja, California Peninsula; Castillo, 2008). HMAs could form by the fractionation of basalts at crustal depths (Humphreys et al., 2006; Chen et al., 2013). Shellnutt and Zellmer (2010) demonstrate that HMAs, which have been regarded as particularly hydrous primary melts generated in equilibrium with mantle peridotite, can form by crystal fractionation from low-H_2O primitive arc basalts in the upper crust as inferred from MELTS modelling. Both of these models may yield the observed EMI-type isotopic compositions of the Daohugou HMAs, with highly fractionated REE patterns, pronounced depletions in HFSEs (e.g., Nb, Ta, and Ti), and enrichments in LILEs relative to LREEs and HFSEs (Fig. 7). The petrogenetic pressure may have influenced the petrogenesis of the Daohugou HMAs. Rhyolite-MELTS modelling indicates that HMAs cannot be produced by fractional crystallization at high pressure (10 kbar) regardless of the relative oxidation state (fO_2) and water content (Fig. 10). Lower pressure (1 kbar) conditions with ~ 4%H_2O content, and higher fO2 (NNO + 2) are better able to produce the Daohugou HMA melts (Fig. 9). Shellnutt and Zellmer (2010) have shown that HMAs may be generated by fractional crystallization at NNO + 2±1 log10 unit. Shallow fractionation is also consistent with the observation that the Daohugou HMAs do not display residual garnet signatures. A relatively high H_2O content is also supported by their mineral composition, with olivine phenocrysts of the Daohugou HMAs having unusually low CaO contents and CaO/FeO ratios (Fig. 2), similar to water-rich subduction-related lavas (Fig. 2; Kamenetsky et al., 2006).

Comparable characteristics are observed in the Xinkailing HMAs, for which the water contents are estimated to be ~6 wt. % and 2.6–6.0 wt. %, respectively, based on the effects of water pressure on mineral/melt partition coefficients for Ca and on the olivine liquidus (Hong et al., 2017). The modelling results predicts the fractionation of about 15% spinel, 3% olivine, and 11% clinopyroxene ($En_{41-45}Fs_{12-15}Wo_{43-44}$) to produce a magma with the composition of the Daohugou HMAs. Early fractionation of spinel-structured oxides is key to the formation of HMAs, as it causes an increase in SiO_2 content and associated depletion of iron oxides, with minimal effect on the remaining major elements, producing HMA melts with 58.5 wt. % SiO_2, 3.5 wt. % MgO. The Daohugou HMAs were therefore most likely derived from shallow-level fractional crystallization from island arc basalts, consequently, crustal differentiation processes may have been important in petrogenesis of HMAs.

The similar isotopic compositions and trace-element pattern of the samples of the present study, combined with the results of quantitative Rhyolite-MELTS modelling, indicate that the samples may be genetically related to each other, and that the magmas which formed the mafic rocks underwent fractionation to produce silicic rocks. The samples show highly fractionated REE patterns with pronounced depletion in HFSE (e.g., Nb, Ta, and Ti) and enrichment in LILE relative to LREE and HFSEs (Fig. 7). Compared with mantle-derived magmatic rocks globally, depletions in Nb, Ta, and Ti are a characteristic of volcanic arc rocks or the “arc signature” exhibited by many continental crustal materials. The negative ε_{Nd} (t) values and variable initial $^{87}Sr/^{86}Sr$ ratios of the samples are consistent with derivation from an EMI-type

isotopically enriched mantle source. EMI-type isotopic compositions are evident in >110 Ma basalts (e.g., Xu, 2001; Zhang et al., 2002; Gao et al., 2008; Yang and Li, 2008; Meng et al., 2015) and HMAs (Gao et al., 2004) in the NCC, while the <110 Ma basalts were derived from the asthenosphere (e.g., the Jianguo basalts; Zhang et al., 2003). Combined with the results of Rhyolite-MELTS modelling, the parental melt was most likely hydrous and formed in a subduction-zone setting. Hydrous SiO_2-rich fluids or melts released from the subducted slab would have reacted with peridotite in the mantle wedge and induced partial melting, with the melts being enriched in LILEs but depleted in HFSEs (e.g., Nb, Ta and Ti).

The sub-continental mantle lithosphere (SCLM) may become enriched in incompatible elements through protracted mantle metasomatism (O'Reilly and Griffin, 1988). Such metasomatism would not significantly affect major elements, but may result in enrichments in volatiles and the more incompatible elements, leading to enriched isotopic signatures (Niu, 2005). A series of successive subduction events have occurred near the eastern NCC since the Paleozoic, resulting in the addition of large amounts of water into the overlying SCLM (Windley et al., 2010). This is indicated by the presence of early Cretaceous mafic lavas at the northern, eastern, and southeastern margins of the NCC that originated from a hydrous SCLM (e.g., Xia et al., 2013; Ma et al., 2016; Hong et al., 2017).

In summary, the Daohugou HMAs may have formed by upper-crustal crystal fractionation of arc basalt derived from metasomatized lithospheric mantle.

5.3 Geodynamic significance

The ancient, cratonic mantle lithosphere, similar to that present beneath the Kaapvaal, Siberian, and other Archean cratons, in inferred to have been removed from the base of the Eastern Block of the NCC in the Mesozoic, and was partly replenished with younger, less refractory lithospheric mantle (Menzies et al., 1993; Griffin et al., 1998; Menzies and Xu, 1998; Zheng, 1999; Fan et al., 2000; O'Relly et al., 2001; Xu, 2001; Zheng et al., 2001, 2007; Gao et al., 2002, 2004; Zhang et al., 2003, ;). As a consequence, the composition, thermal structure, and thickness of the sub-continental lithospheric mantle (SCLM) of the North China Craton have changed dramatically. However, the mechanisms of this process remain controversial.

The "arc-like", EMI Sr–Nd isotopic compositions, the composition of olivine, and the results of Rhyolite-MELTS modelling lead to the conclusion that the Daohugou HMAs were produced by upper-crustal fractional crystallization of arc basalt derived from a metasomatized mantle wedge. Previous studies have suggested a hydrous lithosphere, based on the high water content of early Cretaceous mafic lava and HMAs at the southeastern, eastern, and northern margins of the NCC (Xia et al., 2013; Ma et al., 2016; Hong et al., 2017).

The final closure of the Paleo-Asian Ocean between the North China Craton and Siberian Craton took place in the late Permian (Xiao et al., 2003; Xu B et al., 2013), and eastern China has been affected by subduction of the Paleo-Pacific Plate since the late Mesozoic (Zhao et al., 1994; Niu, 2005). Successive subduction events around the eastern NCC may have introduced large amounts of water into the overlying SCLM (Zhang et al., 2003; Windley et al., 2010), resulting in the production of hydrous

melts that ascended, weakening the base of the lithosphere and, converting basal lithospheric mantle into asthenospheric mantle (Niu, 2005). These hydrous melts re-fertilized the overlying SCLM (Tang et al., 2013; Hong et al., 2017), possibly accelerating the removal of the SCLM, and leading to destabilization of the craton (Zhu et al., 2012; Wang et al., 2015).

6. Conclusions

Mineral chemistry, geochronology, major- and trace-element compositions and Sr–Nd isotopic compositions of the Mesozoic lavas in Inner Mongolia lead to the following conclusions.

1) Zircon U–Pb dating of a Daohugou rhyolite yields an age of 164 ± 1Ma, suggesting that the Daohugou volcanic sequence is coeval with the Tiaojishan Formation in northern Hebei and western Liaoning.

2) The Daohugou volcanic rock suite constitutes a complete compositional spectrum from basaltic trachyandesite to rhyolite. All the rocks are enriched in LILEs and LREEs, and depleted in HFSEs, with similar EMI-type Sr–Nd isotopic compositions.

3) All samples have similar isotopic compositions, and trace-element systematics, consistent with a genetic link by shallow-level (at 1kbar pressure) fractional crystallization.

4) Samples containing <60 wt. % SiO_2 have the characteristics of HMAs, with high MgO, Cr, and Ni contents. The results of MELTs modeling predicts the fractionation of about 15% spinel, 3% olivine, and 11% clinopyroxene

($En_{41-45}Fs_{12-15}Wo_{43-44}$), to yield the magmatic composition of the Daohugou HMAs under conditions of low pressure (1 kbar), a high H_2O content (4 wt. %), and high fO_2 (NNO+2). This indicates upper-crustal fractionation of arc basalt derived from metasomatized lithospheric mantle.

5) The addition of "water" to the cratonic keel may have played a major role in the destruction of the NCC.

Acknowledgements

We are grateful to Drs. R.X. Zhu, F.Y. Wu, Y.B. Wu, Y.X. Pan, H.Y. He for their help during field work, and H. L. Yuan, X. M. Liu, C. L. Zong, M. N. Dai, Y. Liu, J. Q. Wang for their help during the chemical separation and analyses. This study is supported by the National Nature Science Foundation of China (Grants 41273013, 41472155), Scientific Research Foundation of Shandong University of Science and Technology for Recruited Talents (2016RCJJ008), and SDUST Research Fund (No. 2015TDJH101).

References

Black, L.P., Kamo, S. L., Allen, C. M., Aleinikoff, J. N., Davis, D. W., Korsch, R. J., Foudoulis, C., 2003. TEMORA 1: a new zircon standard for Phanerozoic U–Pb geochronology. Chemical Geology 200, 155–170.

Calmus, T., Aguillón-Robles, A., Maury, R. C., Bellon, H., Benoit, M., Cotten, J., Bourgois, J., Michaud, F., 2003. Spatial and temporal evolution of basalts and

magnesian andesites ("bajaites") from Baja California, Mexico: the role of slab melts. Lithos 66, 77-105.

Castillo, P. R., 2008. The origin of the adakite—high-Nb basalt association and its implications for post-subduction magmatism in Baja California, Mexico. Geological Society of America Bulletin 120, 451-462.

Castillo, P. R., 2012. Adakite petrogenesis. Lithos, 134-135: 304-316.

Chen, B., Jahn, B. M., Suzuki, K., 2013. Petrological and Nd-Sr-Os isotopic constraints on the origin of high-Mg adakitic rocks from the North China Craton, tectonic implications. Geology 41, 91–94.

Chen, W., Ji, Q., Liu, D. Y., Zhang, Y., Song, B., Liu, X. Y., 2004. Isotope geochronology of the fossil-bearing beds in the Daohugou area, Ningcheng, Inner Mongolia. Geological Bulletin of China 23, 1165-1169.

Chen, X., Wang, D., Wang, X. L., Gao, J. F., Shu, X. J., Zheng, J. C., Qi, L., 2014. Neoproterozoic chromite-bearing high-Mg diorites in the western part of the Jiangnan orogen, southern China: Geochemistry, petrogenesis and tectonic implications. Lithos 200-201, 35-48.

Chung, S. L., Liu, D. Y., Ji, J. Q., Chu, M. F., Li, H. Y., Wen, D. J., Lo, C. H., Li, T. Y., Qian, Q., Zhang, Q., 2003. Adakites from continental collision zones: melting of thickened lower crust beneath southern Tibet. Geology 31, 1021-1024.

Defant, M. J., Drummond, M. S., 1990. Derivation of some modern arc magmas by melting of subducted lithosphere. Nature 347, 662-665.

Drummond, M. S., Defant, M. J., 1990. A model for trondhjemite-tonalite-dacite genesis and crustal growth via slabs melting: Archean to modern comparisons. Journal of Geophysical Research 95, 21503-21521.

Fan, W. M., Zhang, H. F., Baker, J., Jarvis, K. E., Mason, P. R. D., Menzies M. A., 2000. On and off the North China Craton: Where is the Archaean keel? Journal of Petrology 41, 933-950.

Gao, S., Rudnick, R. L., Carlson, R. W., McDonough, W. F., Liu, Y. S., 2002. Re–Os evidence for replacement of ancient mantle lithosphere beneath the North China Craton. Earth and Planetary Science Letters 198, 307-322.

Gao, S., Rudnick R. L., Yuan, H. L., Liu, X. M., Liu, Y. S., Xu, W. L., Ling, W. L., Ayers, J., Wang, X. C., Wang, Q. H., 2004. Recycling lower continental crust in the North China Craton. Nature 432, 892-897.

Gao, S., Rudnick, R. L., Xu, W. L., Yuan, H. L., Liu, Y. S., Walker, R. J., Puchtel, I. S., Liu, X. M., Huang, H., Wang, X. R., Yang J., 2008. Recycling deep cratonic lithosphere and generation of intraplate magmatism in the North China Craton. Earth and Planetary Science Letters 270, 41-53.

Gualda, G. A. R., Ghiorso, M. S., 2015. MELTS_Excel: A Microsoft Excel-based MELTS interface for research and teaching of magma properties and evolution. Geochemistry, Geophysics, Geosystems doi: 10.1002/2014GC005545.

Green, T.H., Pearson, N.J., 1987. An experimental study of Nb and Ta partitioning between Ti-rich minerals and silicate liquids at high pressure and temperature. Geochimica et Cosmochimica Acta 51, 55-62.

Griffin, W. L., Zhang, A. D., O'Reilly, S. Y., Ryan C. G., 1998. Phanerozoic evolution of the lithosphere beneath the Sino-Korean Craton. In: Flower M. F. J., Chung S. L., Lo C. H., T. Y. Lee eds Mantle Dynamics and Plate Interactions in East Asia. American Geophysical Union, Geodynamics Series 27, 107-126.

Grove, T.L., Baker, M.B., Price, R.C., Parman, S.W., Elkins-Tanton, L.T., Chatterjee, N. & Müntener, O., 2005. Magnesian andesite and dacite lavas from Mt. Shasta, northern California: products of fractional crystallization of H_2O-rich mantle melts. Contributions to Mineralogy and Petrology 148, 542–565.

He, H. Y., Wang, X. L., Zhou, Z. H., Zhu, R. X., Jin, F., Wang., F., Ding, X., Bowen, A., 2004. $^{40}Ar/^{39}Ar$ dating of ignimbrite from Inner Monogolia, northeastern China, indicates a post-Middle Jurassic age for the overlying Daohugou Bed. Geophysical Research Letters 31, L20609.

Hirose, K., 1997. Melting experiments on lherzolite KLB-1 under hydrous conditions and generation of high-magnesian andesitic melts. Geology 25, 42-44.

Hong, L. B., Zhang, Y.H., Xu, Y.G., Ren, Z.Y., Yan, W., Ma, Q., Ma, L., Xie, W., 2017. Hydrous orthopyroxene-rich pyroxenite source of the Xinkailing high magnesium andesites, Western Liaoning: Implications for the subduction-modified lithospheric mantle and the destruction mechanism of the North China Craton. Lithos 282-283, 10-22.

Huang, F., Li, S. G., Dong, F., He, Y. S., Chen, F. K., 2008. High-Mg adakitic rocks in the Dabie orogen, central China: implications for foundering mechanism of lower continental crust. Chemical Geology 255, 1-13.

Humphreys, M.C.S., Blundy, J.D., Sparks, R.S.J., 2006. Magma evolution and open-system processes at Shiveluch volcano: insights from phenocryst zoning. Journal of Petrology 47, 2303–2334.

Jahn, B. M., Wu, F., Lo, C. H., Tsai, C. H., 1999. Crust–mantle interaction induced by deep subduction of the continental crust: geochemical and Sr-Nd isotopic evidence from post-collisional mafic-ultramafic intrusions of the northern Dabie complex. Chemical Geology 157, 119-146.

Ji, Q., Yuan, C. X., 2002. Discovery of two kinds of protofeathered Pterosaurs in the Mesozoic Daohugou biota in the Ningcheng region and its stratigraphic and biologic significances. Geological review 48, 221-224.

Kay, R. W., 1978. Aleutian magnesian andesites: melts from subducted Pacific Ocean crust. Journal of Volcanology and Geothermal Research 4, 117-132.

Kay, R. W., Kay, S. M., 1993. Delamination and delamination magmatism. Tectonophysics 219, 177-189.

Kelemen, P. B., 1995. Genesis of high Mg# andesites and the continental crust. Contributions to Mineralogy and Petrology 120, 1-19.

Le Maitre, R. W., Bateman, P., Dubek, A., Keller, J., Lameyre, J., Le Bas, M. J., Sabine, P. A., Schimid, R., Sorensen, H., 1989. A Classification of Igneous Rocks and Glossary of Terms: Recommendations of the International Union ofGeological Sciences Subcommission the Systematics of Igneous Rocks. Blackwell, Oxford.

Li, S. G., Xiao, Y., Liou, D., Chen, Y., Ge, N., Zhang, Z., Sun, S. S., Cong, B., Zhang,

R., Hart, S. R., Wang, S., 1993. Collision of the North China and Yangtze Blocks and formation of coesite-bearing eclogites: timing and processes. Chemical Geology 109, 89-111.

Liu, D. Y., Nutman, A. P., Compston, W., Wu, J. S., Shen, Q. H., 1992. Remnants of 3800 Ma crust in the Chinese part of the Sino–Korean craton. Geology 20, 339-342

Liu, D. Y., Wilde, S. A., Wan, Y. S., Wu, J. S., Zhou, H. Y., Dong, C. Y., Yin, X. Y., 2008. New U-Pb and Hf isotopic data confirm Anshan as the oldest preserved segment of the North China Craton. American Journal of Science 308, 200-231.

Liu, Y. Q., Liu, Y. X., Ji, S. A., Yang, Z. Q., 2006. SHRIMP U-Pb zircon age for the Daohugou Biota at Ningcheng of Inner Mongolia and comments on related issues. Chinese Science Bulletin 51, 2273-2282.

Liu, Y. S, Wang, X. H, Wang, D., He, D., Zong, K., Gao, C., Hu, Z., Gong, H., 2012. Triassic high-Mg adakitic andesites from Linxi, Inner Mongolia: insights into the fate of the Paleo-Asian ocean crust and fossil slab-derived melt-peridotite interaction. Chemical Geology 328, 89-108.

Ludwig, K. R., 2003. ISOPLOT 3.0: A Geochronological Toolkit for Microsoft Excel. Berkeley: Berkeley Geochronology Center Special Publication 1-70.

Ma, Q., Xu, Y.G., Zheng, J.P., Griffin, W.L., Hong, L.B., Ma, L., 2016. Coexisting early Cretaceous high-Mg andesites and adakitic rocks in the North China Craton: the role of water in interaplate magmatism and cratonic destruction. Journal of Petrology 57, 1279–1308.

Martin, H., Smithies, R. H., Rapp, R., Moyen, J. F., Champion, D., 2005. An overview of adakite, tonalite-trondhjemite-granodiorite (TTG), and sanukitoid: relationships and some implications for crustal evolution. Lithos 79, 1-24.

Meng, F., X., Gao, S., Niu, Y. L., Liu, Y. S., Wang, X.R., 2015. Mesozoic–Cenozoic mantle evolution beneath the North China Craton: A new perspective from Hf–Nd isotopes of basalts. Gondwana Research 27, 1574-1585.

Meng, Q. R., Zhang, G. W., 2000. Geologic framework and tectonic evolution of the Qinling orogen, central China. Tectonophysics 323, 183-196.

Menzies, M. A., Fan, W. M., Zhang M., 1993. Paleozoic and Cenozoic lithoprobes and the loss of >120 km of Archean lithosphere, Sino-Korean craton, China. In: Prichard, H. M., labaster, H. M. A., Harris, T., Neary C. R. eds *Magmatic Processes and Plate Tectonics* 71-81.

Menzies, M. A., Xu, Y. G., 1998. Geodynamics of the North China Craton. In: Flower, M. F. J., Chung, S. L., Lo, C. H., Lee T. Y. eds *Mantle Dynamics and Plate* Interactions in East Asia. American Geophysical Union, Geodynamics Series 27, 155-165.

Niu, Y. L., 2005. Generation and evolution of basaltic magmas: Some basic concepts and a new view on the origin of Mesozoic-Cenozoic basaltic volcanism in Eastern China. Geological Journal of China Universities 11, 9-46.

O'Reilly, S. Y., Griffin, W. L., Poudjom Djomani, Y. H., Morgan, P., 2001. Are lithospheres forever? Tracking changes in sub-continental lithospheric mantle through time. GSA Today 11(4), 4-10.

Plank, T., Langmuir, C. H., 1998. The chemical composition of subducting sediment and its consequences for the crust and mantle. Chemical Geology 145, 325-394.

Qian, Q., Hermann, J., 2010. Formation of high-Mg diorites through assimilation of peridotite by monzodiorite magma at crustal depths. Journal of Petrology 51, 1381-1416.

Rapp, R. P., Norman, M. D., Laporte, D., Yaxley, G. M., Martin, H., Foley, S. F., 2010. Continental formation in the Archean and chemical evolution of the cratonic lithosphere: Melt-rock reaction experiments at 3-4GPa and petrogenesis of Archean Mgdiorites. Journal of Petrology 52, 1237-1266.

Rudnick, R. L., Gao, S., Ling, W. L., Liu, Y. S., McDonough, W. F., 2004. Petrology and geochemistry of spinel peridotite xenoliths from Hannuoba and Qixia, North China Craton. Lithos 77, 609-637.

Santosh, M., 2010. Assembling North China Craton within the Columbia supercontinent: the role of double-sided subduction. Precambrian Research 178, 149-167.

Sato, M., Shuto, K., Nohara-Imanak, R., Takazawa, E., Osanai, Y., Nakano, N., 2014. Repeated magmatism at 34 Ma and 23-20 Ma producing high magnesian adakitic andesites and transitional basalts on southern Okushiri Island, NE Japan arc. Lithos 205, 60-83.

Sengör, A. M. C., Natal'in, B. A., Burtman, V. S., 1999. Evolution of the altaid tectonic collage and Palaeozoic crustal growth in Eurasia. Nature 364, 299-307.

Shellnutt, J. G., Zellmer, G. F., 2010. High-Mg andesite genesis by upper crustal

differentiation. Journal of the Geological Society, London 167, 1081–1088.

Shirey, S. B., Hanson, G. N., 1984. Mantle-derived Archaean monozodiorites and trachyandesites. Nature 310, 222-224.

Song, B., Nutman, A. P., Liu, D. Y., Wu, J. S., 1996. 3800 to 2500 Ma crust in the Anshan area of Liaoning Province, northeastern China. Precambrian Research 78, 79-94.

Streck, M. J., Leeman, W. P., Chesley, J., 2007. High-magnesian andesite from Mount Shasta: A product of magma mixing and contamination, not a primitive mantle melt. Geology 35, 351-354.

Sun, S. S., McDonough, W. F., 1989. Chemical and isotopic systematics of oceanic basalt: implications for mantle composition and processes. In: Saunders, A.D., Norry, M.J. eds., Magmatism in the Ocean Basins. London: Geological Society Special Publication 42, 528-548.

Tatsumi, Y., 1981. Melting experiments on a high-magnesium andesite. Earth and Planetary Science Letters 54, 357-365.

Taylor, S. R., McLennan, S. M., 1985. The Continental Crust: Its Composition and Evolution. Oxford: Blackwell Scientific Publication.

Wang, B., Zhang, H. C., Fang, Y., 2006. Some Jurassic Palaeontinidae (Insecta, Hemiptera) from Daohugou, Inner Mongolia, China. Palaeoworld 15, 115-125.

Windley, B. F., Maruyama, S., Xiao, W.J., 2010. Delamination/thinning of sub-continental lithospheric mantle under Eastern China, the role of water and multiple subduction. American Journal of Science 310, 1250-1293.

Workman, R. K., Hart, S. R., 2005. Major and trace element composition of the depleted MORB mantle (DMM). Earth and Planetary Science Letters 231, 53-72.

Xia, Q. K., Liu, J., Liu, S.C., Kovacs, I., Feng, M., Dang, L., 2013. High water content in Mesozoic primitive basalts of the North China Craton and implications on the destruction of cratonic mantle lithosphere. Earth and Planetary Science Letters 361, 85–97.

Xiao, W. J., Windley, B. F., Hao, J., Zhai, M. G., 2003. Accretion leading to collision and the Permian Solonker Suture, Inner Mongolia, China: termination of the central Asian orogenic belt. Tectonics 22, 1069. doi: 10.1029/2002TC001484.

Xu, B., Charvet, J., Chen, Y., Zhao, P., Shi, G. Z., 2013. Middle Paleozoic convergent orogenic belts in western Inner Mongolia (China): framework, kinematics, geochronology and implications for tectonic evolution of the Central Asian Orogenic Belt. Gondwana Research 23, 1342-1364.

Xu, J. F., Shinjo, R., Defant, M. J., Wang, Q., Rapp, R. P., 2002. Origin of Mesozoic adakitic intrusive rocks in the Ningzhen area of east China: partial melting of delaminated lower continental crust? Geology 30, 1111-1114.

Xu, Y. G., 2001. Thermo-tectonic destruction of the Archean lithospheric keel beneath the Sino-Korean Craton in China: evidence timing and mechanism. Physics and Chemistry of the Earth (A) 26, 747-757.

Yang, W., Li, S. G., 2008. Geochronology and geochemistry of the Mesozoic volcanic rocks in Western Liaoning: Implications for lithospheric thinning of the North China Craton. Lithos 102, 88-117.

Zhai, M. G., Santosh M., 2011. The Early Precambrian odyssey of the North China Craton: a synoptic overview. Gondwana Research 20, 6-25

Zhang, H. F., Sun, M., Zhou, X. H., Fan, W. M., Zhai, M. G., Yin, J. F., 2002. Mesozoic lithospheric destruction beneath the North China Carton: evidence from major-, trace-element and Sr-Nd-Pb isotope studies of Fangcheng basalts. Contributions to Mineralogy and Petrology 144, 241-253.

Zhang, H. F., Sun, M., Zhou, X., Zhou, M., Fan, W., Zheng, J., 2003. Secular evolution of the lithosphere beneath the eastern North China Craton: evidence from Mesozoic basalts and high-Mg andesites. Geochimica et Cosmochimica Acta 67, 4373-4387.

Zhang, R.X., Yang, S.Y., 2016. A mathematical model for determining carbon coating thickness and its application in electron probe microanalysis. Microscopy and Microanalysis, 22: 1374-1380.

Zhang, Y. Z., Wang, Y. J., Fan, W. M., Zhang, A. M., Ma, L. Y., 2012. Geochronological and geochemical constraints on the metasomatised source for the Neoproterozoic (~825 Ma) high-mg volcanic rocks from the Cangshuipu area (Hunan Province) along the Jiangnan domain and their tectonic implications. Precambrian Research 220-221, 139-157.

Zhao, G. C., Zhai, M. G., 2013. Lithotectonic elements of Precambrian basement in the North China Craton: Review and tectonic implications. Gondwana Research 23, 1207-1240.

Zhao, G. C., Sun, M., Wilde, S. A., Li, S. Z., 2005. Late Archean to Paleoproterozoic

evolution of the North China Craton: key issues revisited. Precambrian Research 136, 177-202.

Zhao, Y., Yang, Z. Y., Ma, X. H., 1994. Geotectonic transition from Paleo-Asian system and Paleo-Tethyan system to Paleo-Pacific active continental margin in eastern Asia. Sci. Geol. Sin. 29, 105-119.

Zheng, J. P., 1999. Mesozoic–Cenozoic mantle replacement and lithospheric thinning, east China. University of Geosciences Press, Wuhan.

Zheng, J. P., O'Reilly, S. Y., Griffin, W. L., Lu, F. X., Zhang, M., Pearson, N. J., 2001. Relict refractory mantle beneath the eastern North China block: significance for lithosphere evolution. Lithos 57, 43-66.

Zheng, J. P., Griffin, W. L., O'Reilly, S. Y., Yu, C. M., Zhang, H. F., Pearson, N., Zhang, M., 2007. Mechanism and timing of lithospheric modification and replacement beneath the eastern North China Craton: peridotitic xenoliths from the 100 Ma Fuxin basalts and a regional synthesis. Geochimica et Cosmochimica Acta 71, 5203-5225.

Zhu, R., Yang, J., Wu, F., 2012. Timing of destruction of the North China Craton. Lithos 149, 51–60.

Zindler, A., Hart, S., 1986. Chemical geodynamics. Annual Review of Earth Planetary Sciences 14, 493-571.

Figure Captions

Fig. 1 (a) Sketch map of the major tectonic divisions of China. WB, TNCO and EB denote the Western Block, Trans-North China Orogen and Eastern Block, respectively, of the North China Craton (Zhao et al., 2005). SC, South China Block; YZ, Yangtze Block. (b) Simplified map of the Ningcheng-Lingyuan Basin. (c,) Simplified geological map showing sample locations of the Daohugou volcanic rocks.

Fig. 2 Olivine compositional diagrams: (a) CaO versus Fo; and (b) 100 CaO/FeO vs. Fo. Pink and gray dashed lines outline the compositional range of olivines in non-subduction-related lavas and subduction-related lavas, respectively (modified after Hong et al., 2017). Data for the Xinkailing HMAs and high-MgO basalts of the Yixian Formation, western Liaoning are from Hong et al. (2017) and Gao et al. (2008).

Fig. 3 Cathodoluminescence (CL) images of representative zircons from the Daohugou rhyolite (sample DHG-57).

Fig. 4 U–Pb concordia diagram for the Daohugou rhyolite (sample DHG-57).

Fig. 5 TAS (Na_2O+K_2O vs. SiO_2) diagram (Le Maitre et al., 1989) showing the compositional variations in Mesozoic volcanic rocks from Daohugou, Ningcheng, Inner Mongolia.

Fig. 6 Major-element vs. SiO_2 variation diagrams for the Daohugou volcanic rocks. $Fe_2O_3^T$ is expressed as total Fe. The data show linear trends except for a sharp decrease in Al_2O_3 and Na_2O contents at SiO_2 contents above ~ 60 wt. %,

indicating the appearance of plagioclase as a liquidus phase.

Fig. 7 (a) Chondrite normalized REE patterns and (b) primitive mantle normalized trace-element patterns for the Daohugou volcanic rocks. Chondrite values are from Taylor and McLennan (1985), and primitive-mantle values are from Sun and McDonough (1989).

Fig. 8 SiO_2 variation diagrams for Sr, Ni, Sr/Y, and $(La/Yb)_N$ ratios in the Daohugou volcanic rocks. The symbols are the same as in Fig. 6. The solid lines represent the fractionation models of primitive high-Mg basaltic composition (sample DHG67) at low pressure (1 kba), high oxygen fugacity (NNO+2), and an initial H_2O contents of 4 wt. %. Tick marks at 20% intervals represent the percentage of crystallization.

Fig. 9 Chemical variations of rock suites including HMAs from the Daohugou area and results of modeling at low pressure (1 kbar). Rhyolite-MELTS fractionation models of primitive high-Mg basaltic composition (sample DHG67) are given at various oxygen fugacities (NNO, NNO+1, NNO+2), and initial H_2O contents of 0.5 wt. % (undersaturated) and 4 wt. % (saturated at 1 kbar). Tick marks at 10% intervals represent the percentage of crystallization.

Fig. 10 Chemical variations in rock suites at high pressure (10 kbar). Rhyolite-MELTS fractionation models of primitive high-Mg basaltic composition (sample DHG67) are given at various oxygen fugacities (NNO, NNO+1, NNO+2), and initial H_2O contents of 0.5 wt. % (undersaturated) and 4 wt. % (undersaturated at 10 kbar). Tick marks at 10% intervals represent the

percentage of crystallization. The results of modeling do not reproduce the HMA compositions.

Fig. 11 Plot of Sr/Y vs. Y (Drummond and Defant, 1990), which is commonlu used to distinguish adakite from normal arc andesite, dacite, and rhyolite (ADR) lavas.

Fig. 12 $\varepsilon_{Nd}(t)$ vs. $(^{87}Sr/^{86}Sr)_i$ diagram for Mesozoic volcanic rocks from Daohugou. Data for LCC (model lower continental crust), GLOSS (global subducting sediments) and DMM (depleted MORB mantle) are from Jahn et al. (1999), Plank and Langmuir (1998) and Workman and Hart (2005), respectively. The trends for EM-I and EM-II are from Zindler and Hart (1986).

Table 1 Representative Major and trace element data of Daohugou volcanic rocks

	DHG-28	DHG-29	DHG-39	DHG-39R	DHG-40	DHG-58	DHG-59	DHG-62	DHG-62R	DHG-63	DHG-64	DHG-64R	DHG-66	DHG-66R
SiO_2	62.86	63.58	54.64	54.69	55.3	55.27	55.55	59.69	59.71	56.19	54.6	54.55	48.36	
TiO_2	1.20	1.26	1.12	1.14	1.11	1.13	1.12	0.75	0.75	1.02	1.11	1.11	1.79	
Al_2O_3	17.31	17.22	14.91	14.9	14.96	15.14	15.2	15.7	15.72	15.15	15.04	14.99	14.06	
TFe_2O_3	3.97	4.02	8.11	8.15	7.93	8.02	7.73	6.71	6.70	7.60	8.27	8.25	12.36	
MnO	0.05	0.05	0.08	0.08	0.09	0.21	0.10	0.07	0.07	0.09	0.11	0.11	0.15	
MgO	0.52	0.39	4.70	4.68	4.55	3.54	4.12	1.60	1.58	4.50	6.05	6.00	7.44	
CaO	3.27	3.16	5.65	5.67	5.55	5.60	5.79	4.09	4.09	5.52	6.27	6.26	7.54	
Na_2O	5.68	5.57	4.65	4.59	4.65	4.76	4.96	4.76	4.77	4.50	4.01	3.97	4.13	
K_2O	3.29	3.51	3.00	3.00	2.99	3.19	2.37	3.67	3.67	2.98	2.47	2.46	1.64	
P_2O_5	0.43	0.55	0.70	0.72	0.71	0.72	0.72	0.53	0.53	0.63	0.59	0.59	0.99	
LOI	0.96	0.96	2.07	1.99	1.66	1.95	1.87	1.93	1.95	1.33	1.30	1.27	1.49	
SUM	99.54	100.3	99.63	99.61	99.53	99.53	99.5	99.54		99.51	99.82	99.56	99.95	
$Mg^{\#}$	21	16	53	53	53	47	51	32	32	54	59	59	54	
Be	1.64	1.70	2.02	1.98	2.04	2.27	2.07	2.26		1.91	1.68	1.67	1.85	1.75
Sc	12.85	8.56	13.2	13.1	13.2	14.3	13.5	9.60		13.8	16.1	15.7	20.7	19.4
V	34.2	39.6	123	122	124	134	126	94.9		122	132	132	191	183
Cr	2.48	3.39	192	192	198	217	173	90.1		185	214	209	244	235
Co	47.7	35.3	48.4	48.2	80.7	36.9	75.7	34.2		47.1	46.2	45.1	54.2	52.2
Ni	1.69	2.33	77.8	77.8	79.9	81.0	75.3	64.6		80.5	135	135	135	131
Cu	1.99	2.17	33.3	33.2	32.7	36.3	34.0	23.2		34.9	36.4	36.1	54.5	52.6
Zn	109	92.3	98.4	98.4	101	110	99.9	87.2		93.4	88.2	87.8	134	130
Ga	21.9	21.7	20.4	20.5	20.6	21.0	21.0	20.3		20.1	19.0	18.7	20.4	19.6
Rb	79.3	80.0	61.8	61.3	61.8	76.1	48.8	98.8		62.8	50.3	50.2	21.1	19.5
Sr	670	616	1337	1347	1370	1396	1489	1236		1218	958	968	1279	1280
Y	25.4	32.8	17.2	17.1	17.1	17.9	17.6	15.7		17.6	19.1	19.2	24.2	24.1
Zr	266	241	231	232	233	239	239	241		231	197	200	195	196
Nb	12.3	12.0	17.8	17.9	17.9	19.8	19.9	15.3		17.8	18.0	16.9	20.9	19.3
Cs	1.24	0.72	0.44	0.45	0.54	0.98	0.97	1.16		0.41	0.34	0.35	0.95	0.97

Ba	1288	1309	1381	1397	1416	1359	1519	1643	1392	1071	1098	1024	1037
La	43.7	54.1	64.3	65.3	65.4	64.4	66.4	65.9	62.9	47.2	48.6	57.9	58.3
Ce	85.3	90.7	123	126	125	124	129	113	117	93.5	96.6	121	122
Pr	10.5	13.6	13.9	14.0	14.1	13.2	13.7	12.3	12.4	10.2	11.3	13.9	15.2
Nd	43.2	57.2	54.3	55.2	54.3	51.9	53.2	46.3	47.3	40.6	42.2	57.1	59.6
Sm	7.83	10.6	8.37	8.51	8.42	8.07	8.23	7.01	7.30	6.71	7.04	9.64	10.2
Eu	2.34	2.87	2.21	2.25	2.21	2.21	2.24	1.92	2.07	1.89	1.93	2.75	2.74
Gd	6.34	8.64	5.67	5.83	5.77	5.37	5.47	4.70	5.05	4.98	5.19	6.84	7.19
Tb	0.94	1.28	0.77	0.79	0.79	0.72	0.73	0.63	0.69	0.71	0.73	0.95	0.99
Dy	4.62	6.41	3.50	3.63	3.52	3.43	3.50	3.09	3.34	3.60	3.72	4.63	4.89
Ho	0.85	1.20	0.60	0.62	0.60	0.59	0.61	0.56	0.60	0.66	0.68	0.83	0.86
Er	2.28	3.20	1.57	1.64	1.62	1.50	1.53	1.45	1.56	1.73	1.83	2.14	2.24
Tm	0.32	0.45	0.22	0.22	0.22	0.21	0.21	0.22	0.22	0.25	0.27	0.30	0.32
Yb	1.81	2.41	1.26	1.29	1.26	1.24	1.23	1.28	1.31	1.51	1.60	1.73	1.83
Lu	0.26	0.35	0.18	0.19	0.19	0.18	0.18	0.19	0.19	0.22	0.22	0.25	0.26
Hf	5.75	5.77	4.88	5.05	4.93	4.76	5.02	5.24	4.81	4.29	4.42	4.13	4.37
Ta	0.83	0.89	1.08	1.09	1.12	0.91	1.03	0.76	0.89	0.99	1.15	1.03	1.20
Pb	15.0	13.8	12.3	12.6	12.4	11.5	12.4	16.5	12.2	9.76	10.50	6.49	6.78
Th	4.64	5.03	5.24	5.33	5.22	4.97	5.36	6.00	5.08	3.95	4.03	3.04	3.11
U	1.01	1.13	1.09	1.12	1.12	1.00	1.28	1.16	1.03	0.92	0.95	0.70	0.72

Table 2. Sr-Nd isotopic compositions of Daohugou volcanic rocks

Sample	$^{87}Rb/^{86}Sr$	$^{87}Sr/^{86}Sr$		2σ	$^{87}Sr/^{86}Sr$ (t)	$^{147}Sm/^{144}Nd$	$^{143}Nd/^{144}Nd$		2σ	ε_{Nd} (t)
DHG-28	0.3424	0.706662	±	14	0.705883	0.10944	0.511924	±	6	-12.1
DHG-29	0.3760	0.706694	±	20	0.705839	0.11211	0.511944	±	5	-11.8
DHG-39	0.1339	0.705592	±	14	0.705288	0.09314	0.511858	±	9	-13.1
DHG-40	0.1305	0.705582	±	18	0.705285	0.09356	0.511859	±	8	-13.1
DHG-54	0.1532	0.705657	±	17	0.705308	0.09312	0.511852	±	5	-13.2
DHG-58	0.1579	0.705589	±	15	0.705230	0.09389	0.511848	±	9	-13.3
DHG-59	0.0948	0.705539	±	17	0.705324	0.09332	0.511863	±	8	-13.0
DHG-62	0.2314	0.705971	±	17	0.705445	0.09137	0.511735	±	5	-15.4
DHG-63	0.1492	0.705649	±	16	0.705309	0.09309	0.511830	±	10	-13.6
DHG-66	0.0478	0.705450	±	14	0.705341	0.10192	0.511890	±	9	-12.6
DHG-68	0.0714	0.705405	±	17	0.705242	0.10259	0.511880	±	6	-12.8

Highlights

The age of the Daohugou lavas is 164±1Ma and equivalent to the Tiaojishan Formation.

Samples with SiO_2<60 wt. % are similar to high-Mg andesite.

The HMAs are formed by upper crustal fractional crystallization from arc basalt.

The parental melt is derived from an ancient metasomatized lithospheric mantle source.

Addition of “water” to cratonic keel may play a major role in destruction of the NCC.

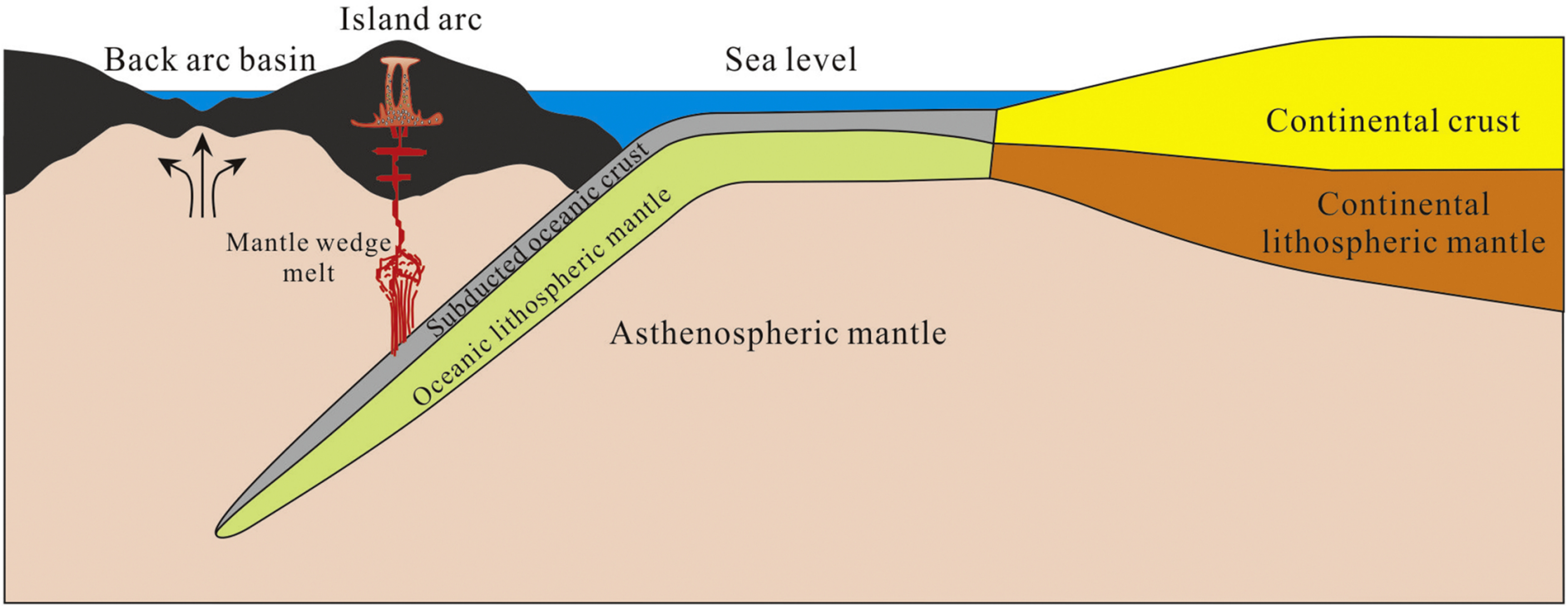

Graphics Abstract

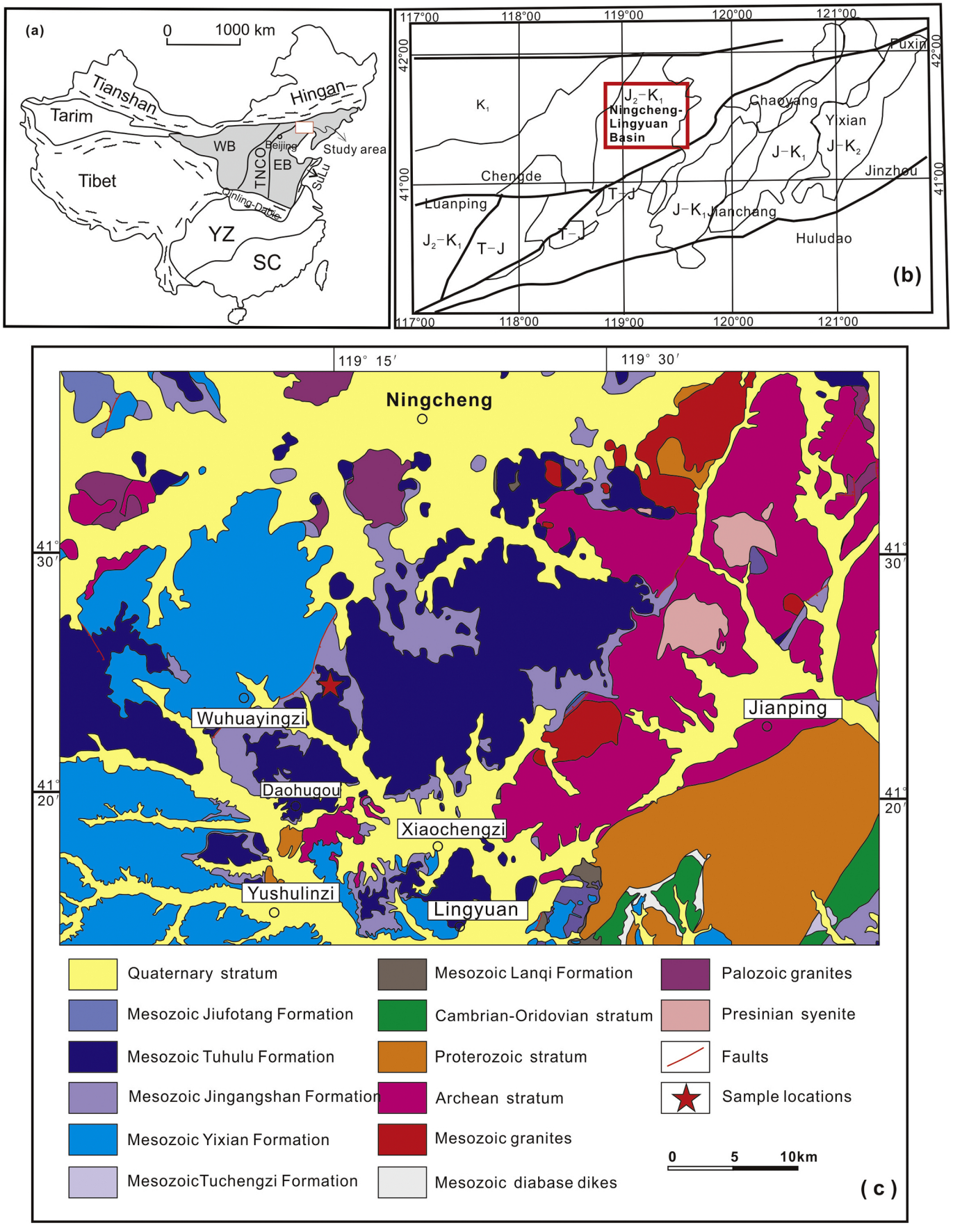
(a)
0 1000 km
Tianshan
Hingan
Tarim
WB
Beijing
Study area
TNCO
EB
Tibet
SuLu
Qinling-Dabie
YZ
SC
(b)
117°00
118°00
119°00
120°00
121°00
42°00
41°00
Fuxin
K1
J2–K1
Ningcheng-
Lingyuan
Basin
Chaoyang
Yixian
J–K1
J–K2
Chengde
Jinzhou
Luanping
T–J
J–K1 Manchang
J2–K1
T–J
T–
Huludao
(b)
119° 15′
119° 30′
41° 30′
41° 20′
Ningcheng
Wuhuayingzi
Jianping
Daohugou
Xiaochengzi
Yushulinzi
Lingyuan
Quaternary stratum
Mesozoic Jiufotang Formation
Mesozoic Tuhulu Formation
Mesozoic Jingangshan Formation
Mesozoic Yixian Formation
MesozoicTuchengzi Formation
Mesozoic Lanqi Formation
Cambrian-Oridovian stratum
Proterozoic stratum
Archean stratum
Mesozoic granites
Mesozoic diabase dikes
Palozoic granites
Presinian syenite
Faults
Sample locations
0 5 10km
(c)

Figure 1

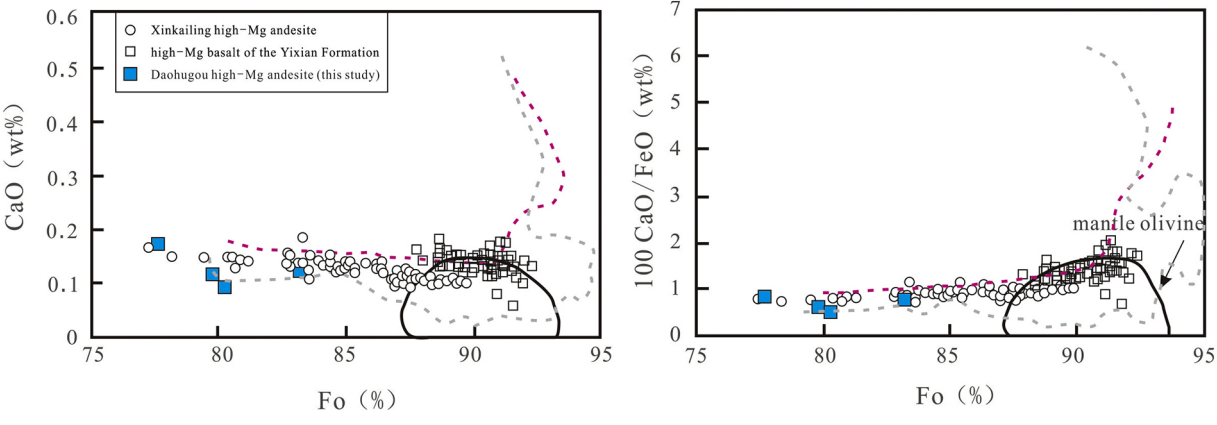
Xinkailing high−Mg andesite
high−Mg basalt of the Yixian Formation
Daohugou high−Mg andesite (this study)
CaO（wt%）
Fo（%）
100 CaO/FeO（wt%）
mantle olivine
Fo（%）

Figure 2

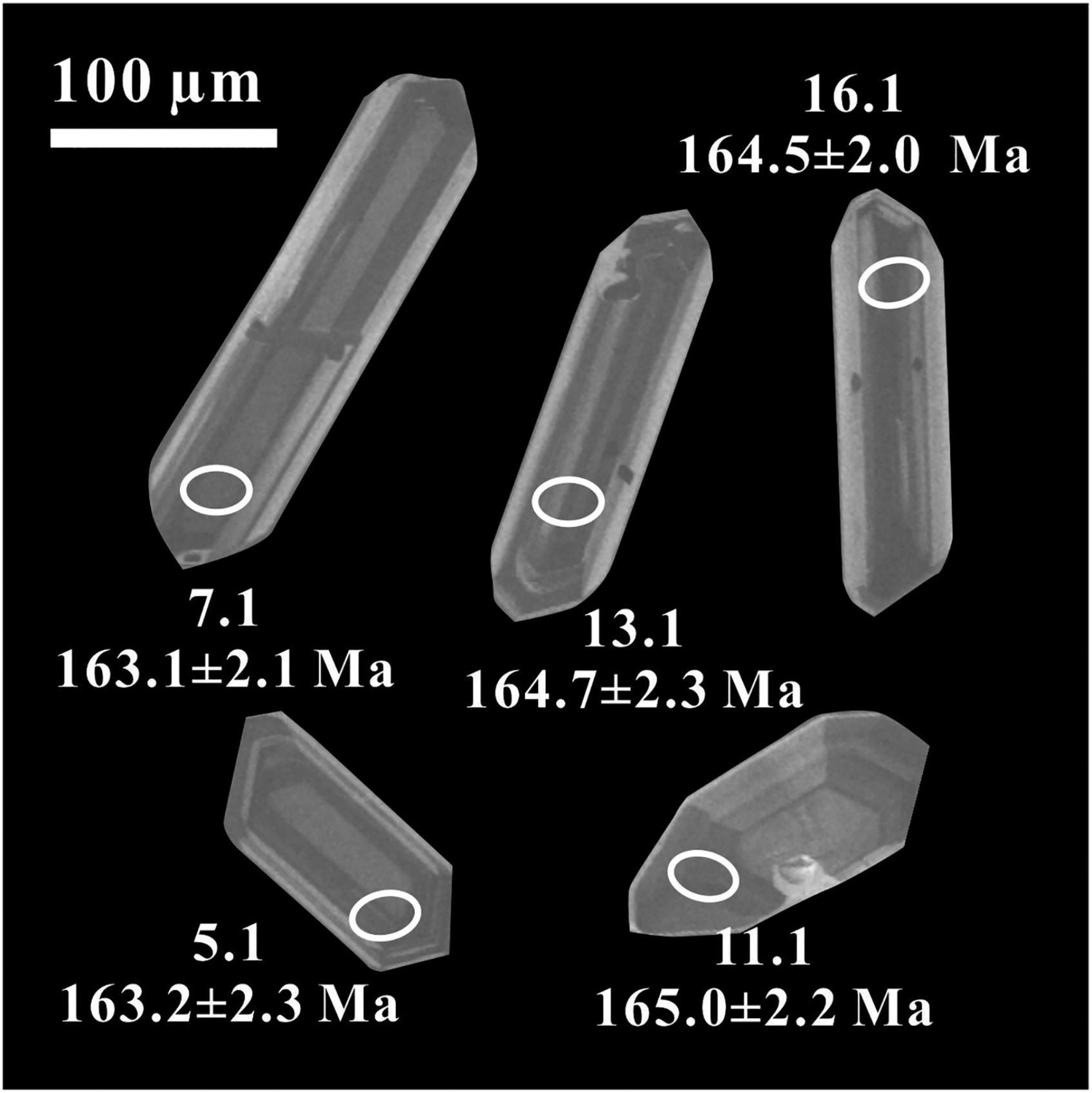
100 µm
16.1
164.5±2.0 Ma
7.1
163.1±2.1 Ma
13.1
164.7±2.3 Ma
5.1
163.2±2.3 Ma
11.1
165.0±2.2 Ma

Figure 3

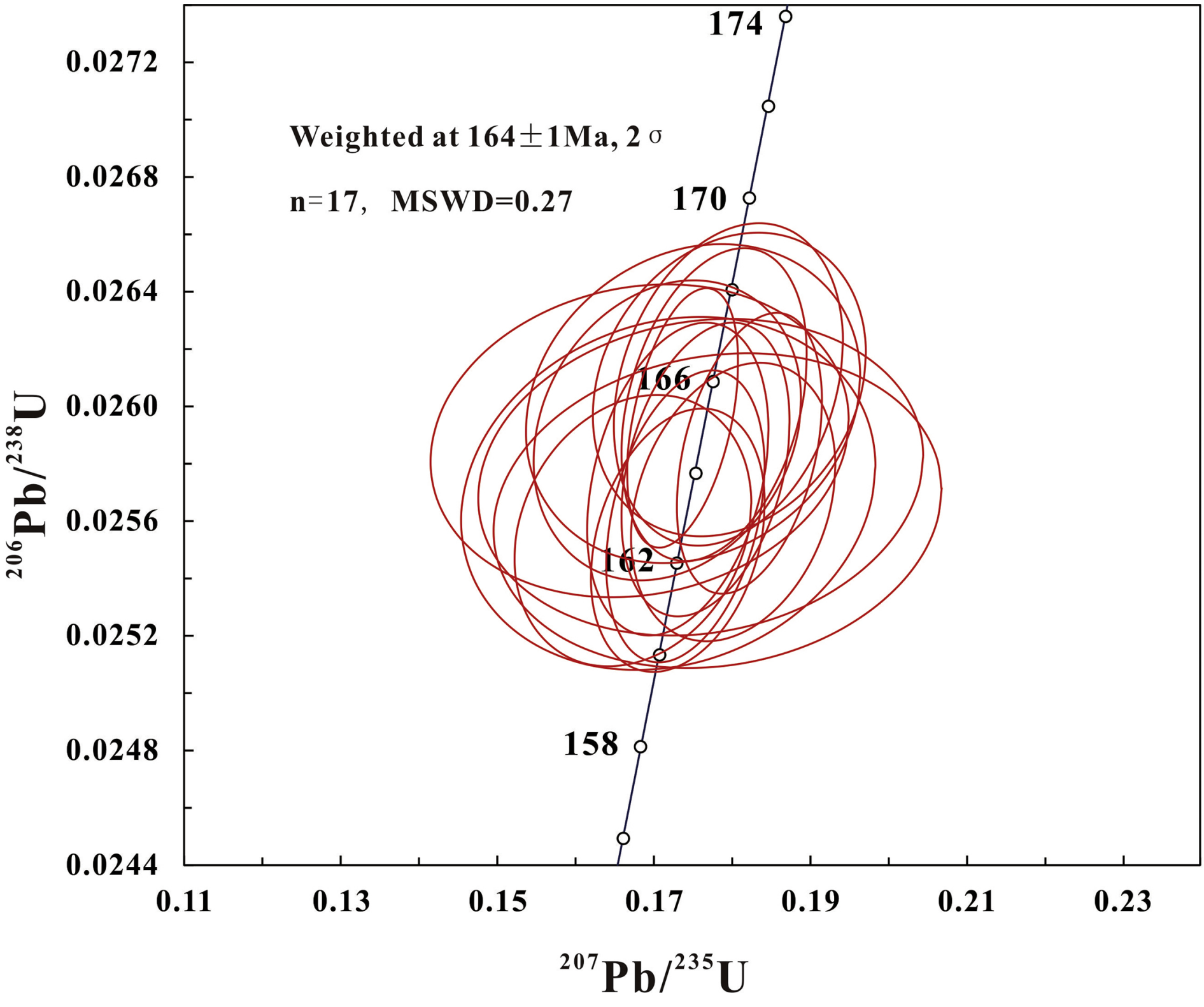
Weighted at 164±1Ma, 2 σ
n=17, MSWD=0.27
174
170
166
162
158
0.0272
0.0268
0.0264
0.0260
0.0256
0.0252
0.0248
0.0244
0.11
0.13
0.15
0.17
0.19
0.21
0.23
$^{206}Pb/^{238}U$
$^{207}Pb/^{235}U$

Figure 4

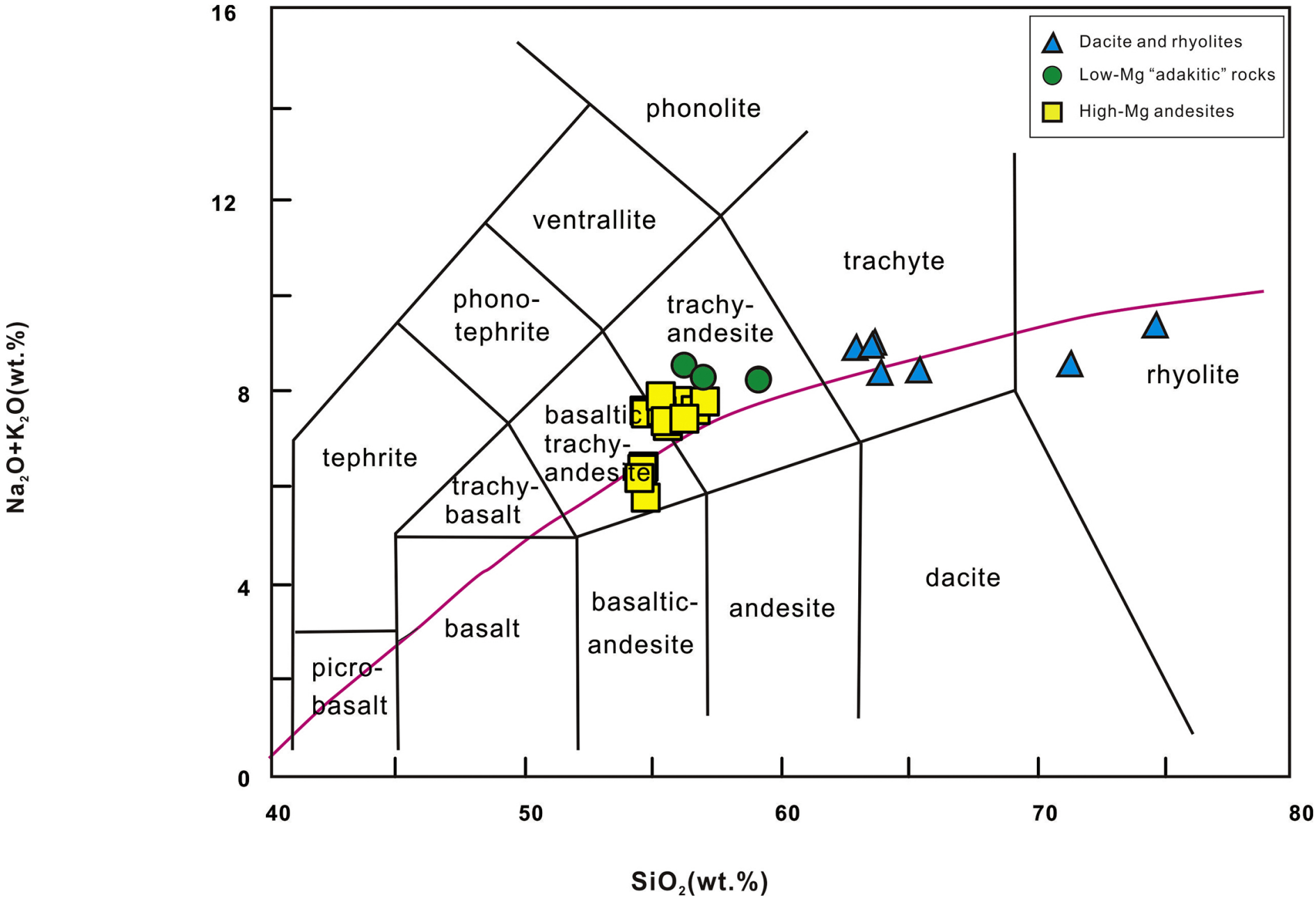
Dacite and rhyolites
Low-Mg "adakitic" rocks
High-Mg andesites
phonolite
ventrallite
phono-
tephrite
trachyte
trachy-
andesite
rhyolite
basaltic
trachy-
andesite
tephrite
trachy-
basalt
dacite
basaltic-
andesite
andesite
basalt
picro-
basalt
16
12
8
4
0
40
50
60
70
80
Na_2O+K_2O(wt.%)
SiO_2(wt.%)

Figure 5

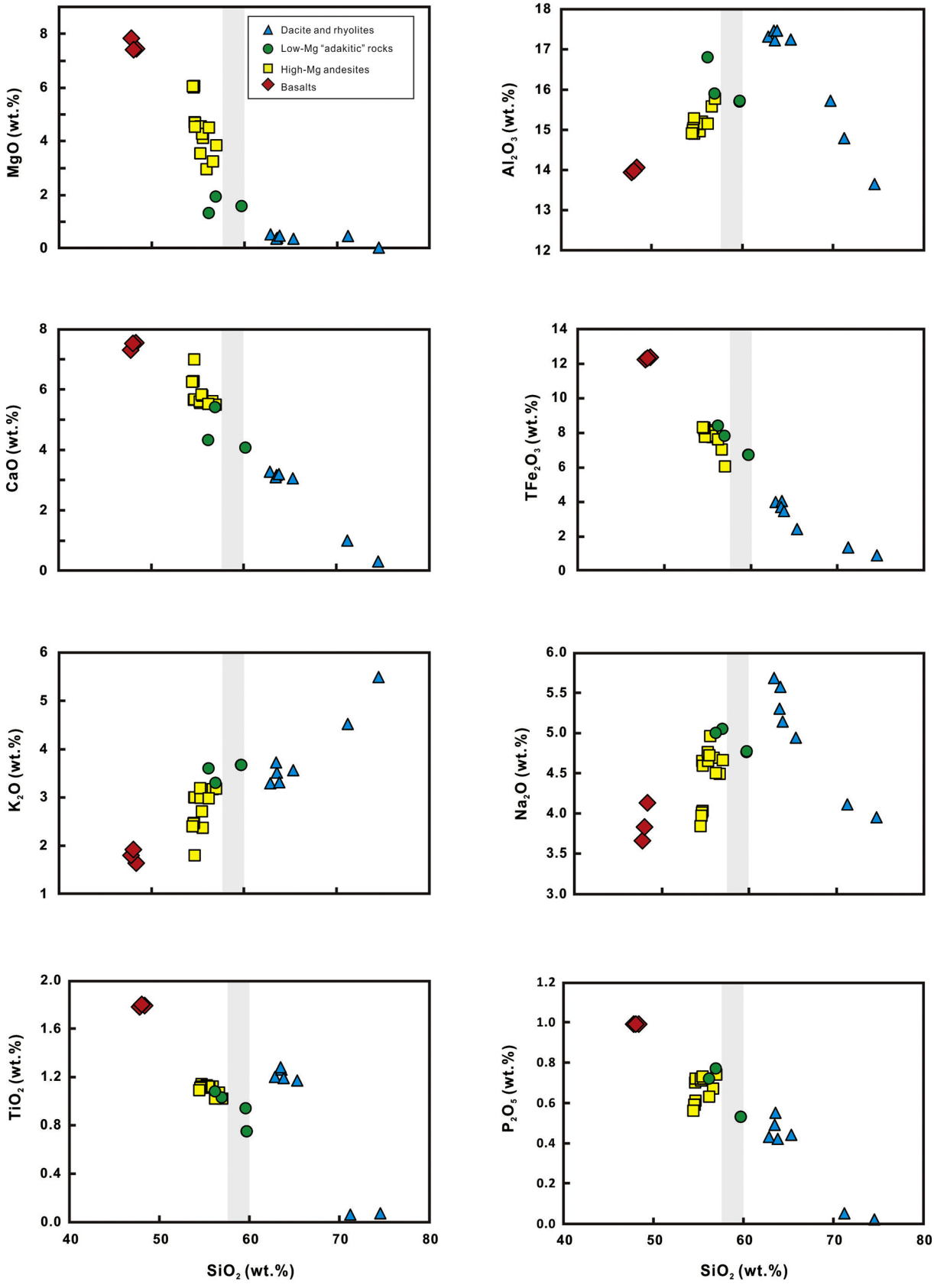
Dacite and rhyolites
Low-Mg "adakitic" rocks
High-Mg andesites
Basalts
MgO (wt.%)
Al2O3 (wt.%)
CaO (wt.%)
TFe2O3 (wt.%)
K2O (wt.%)
Na2O (wt.%)
TiO2 (wt.%)
P2O5 (wt.%)
SiO2 (wt.%)
SiO2 (wt.%)

Figure 6

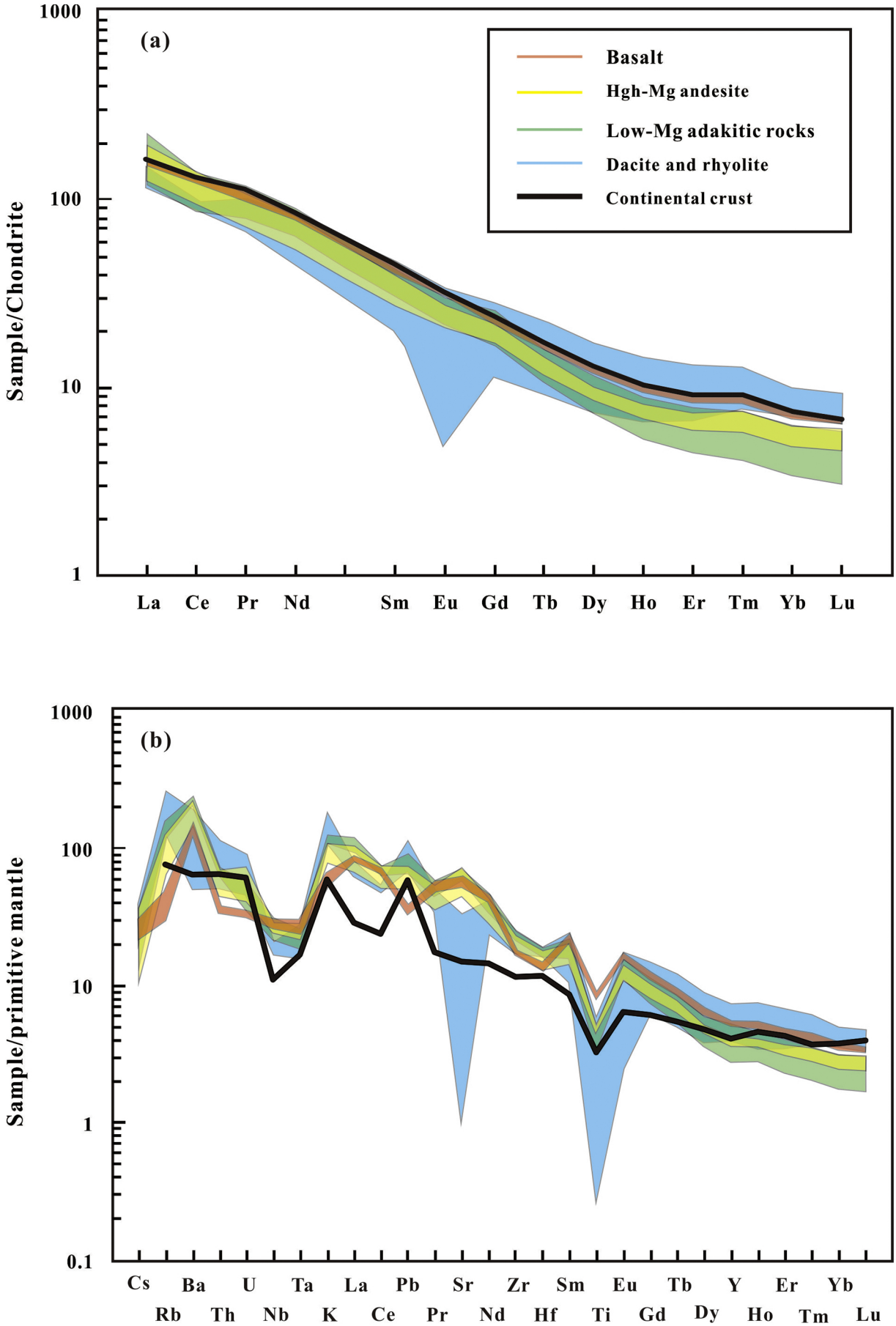
(a)
Basalt
Hgh-Mg andesite
Low-Mg adakitic rocks
Dacite and rhyolite
Continental crust
Sample/Chondrite
1000
100
10
1
La Ce Pr Nd Sm Eu Gd Tb Dy Ho Er Tm Yb Lu
(b)
Sample/primitive mantle
1000
100
10
1
0.1
Cs Rb Ba Th U Nb Ta K La Ce Pb Pr Sr Nd Zr Hf Sm Ti Eu Gd Tb Dy Y Ho Er Tm Yb Lu

Figure 7

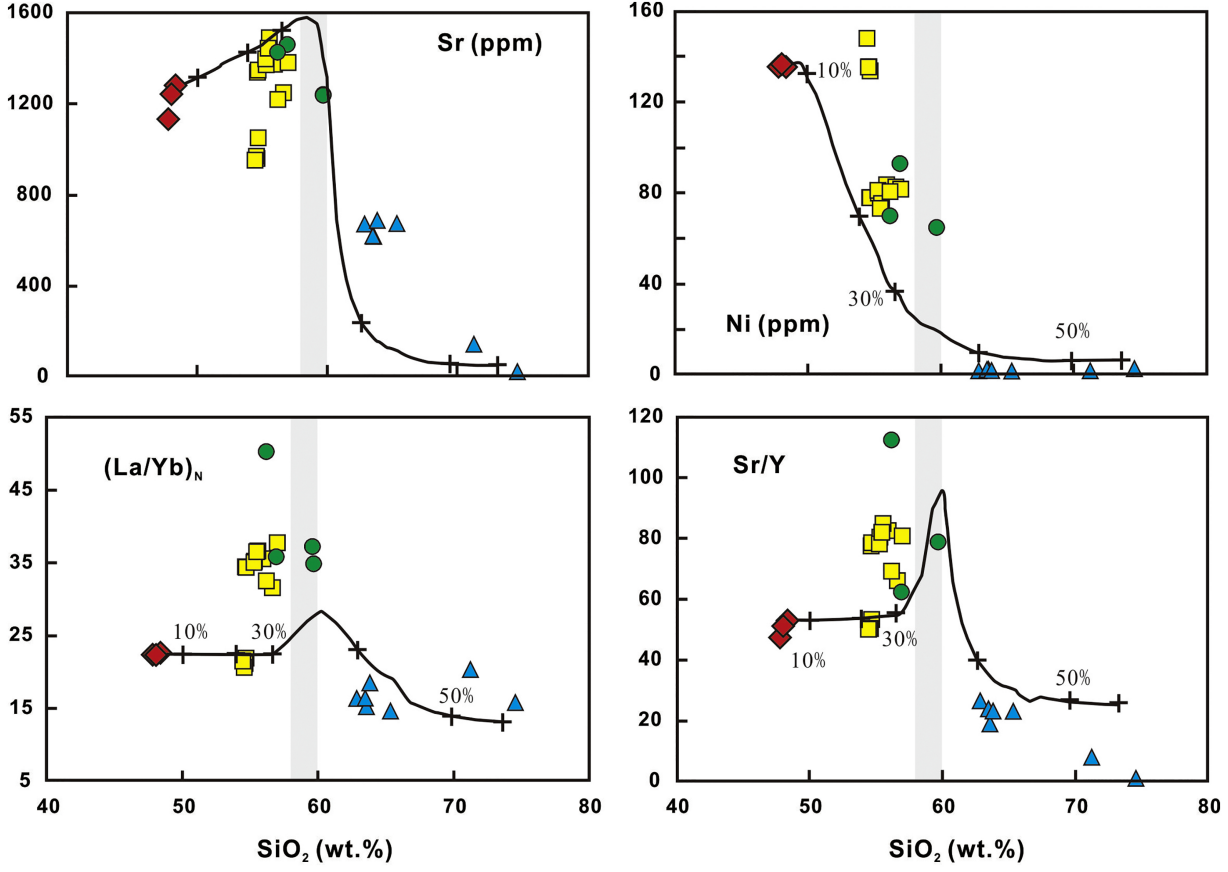
Sr (ppm)
1600
1200
800
400
0
Ni (ppm)
160
120
80
40
0
10%
30%
50%
(La/Yb)N
55
45
35
25
15
5
Sr/Y
120
100
80
60
40
20
0
40
50
60
70
80
SiO2 (wt.%)

Figure 8

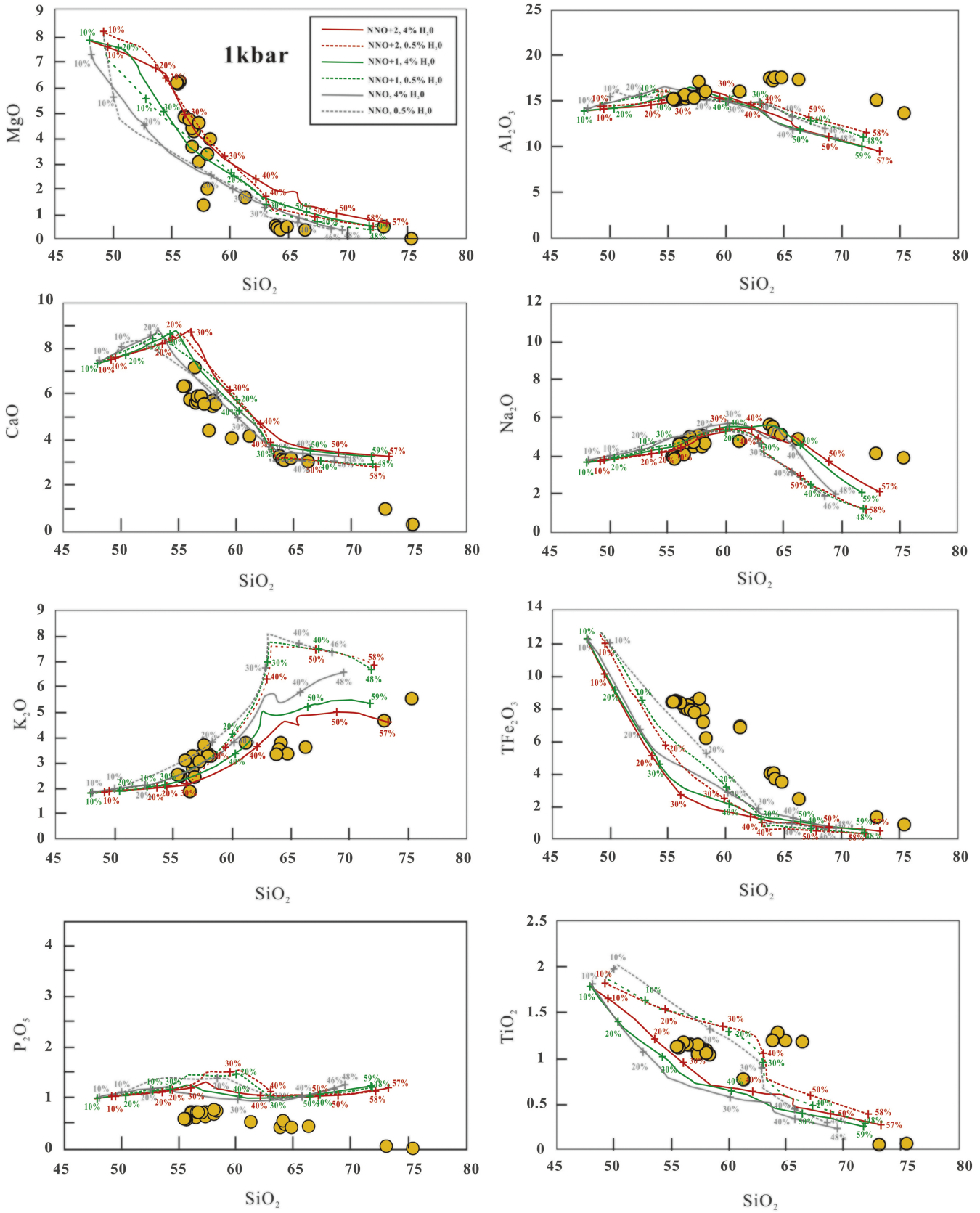
1kbar
NNO+2, 4% H2O
NNO+2, 0.5% H2O
NNO+1, 4% H2O
NNO+1, 0.5% H2O
NNO, 4% H2O
NNO, 0.5% H2O
MgO
Al2O3
CaO
Na2O
K2O
TFe2O3
P2O5
TiO2
SiO2

Figure 9

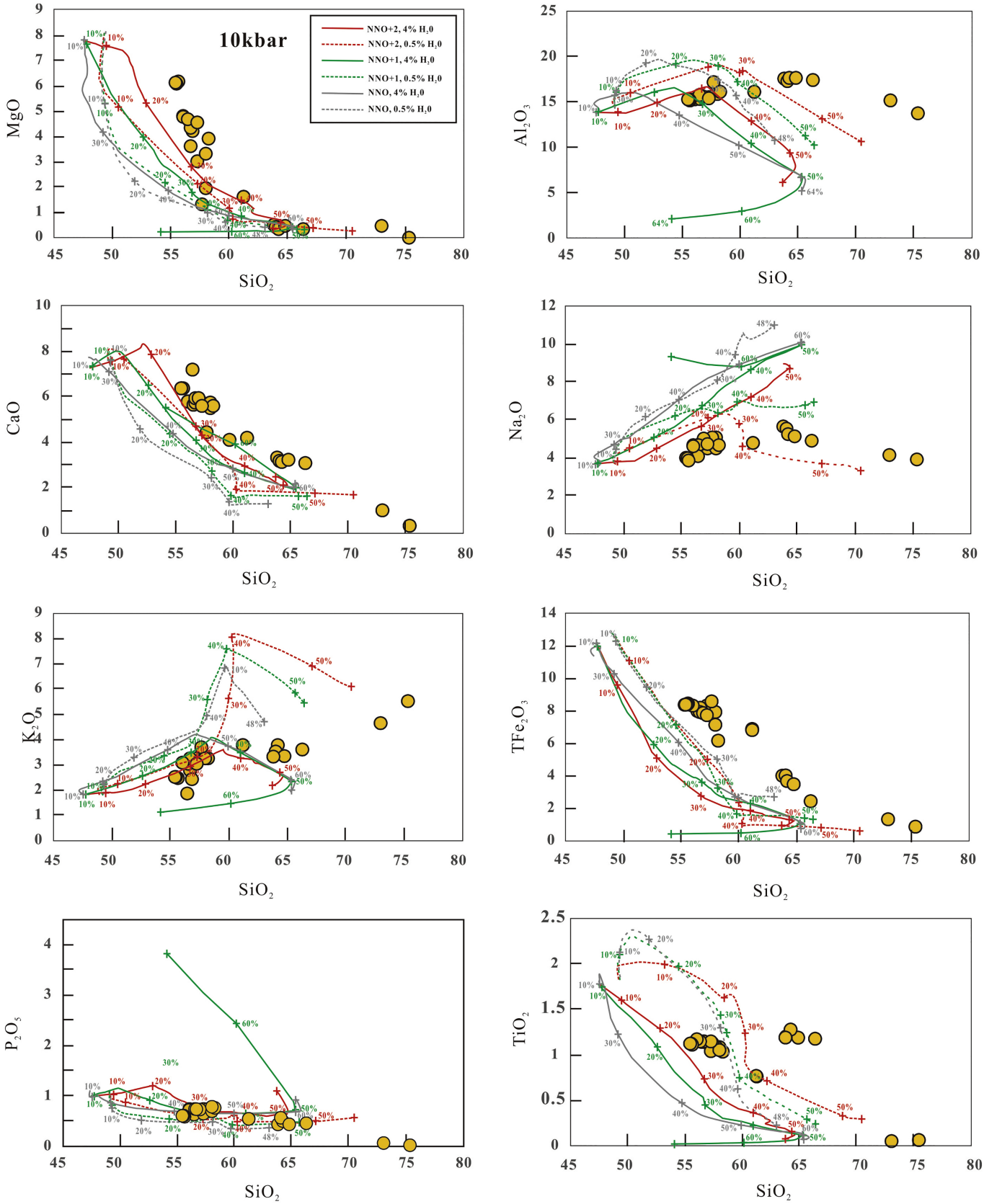
10kbar
NNO+2, 4% H2O
NNO+2, 0.5% H2O
NNO+1, 4% H2O
NNO+1, 0.5% H2O
NNO, 4% H2O
NNO, 0.5% H2O
MgO
Al2O3
CaO
Na2O
K2O
TFe2O3
P2O5
TiO2
SiO2

Figure 10

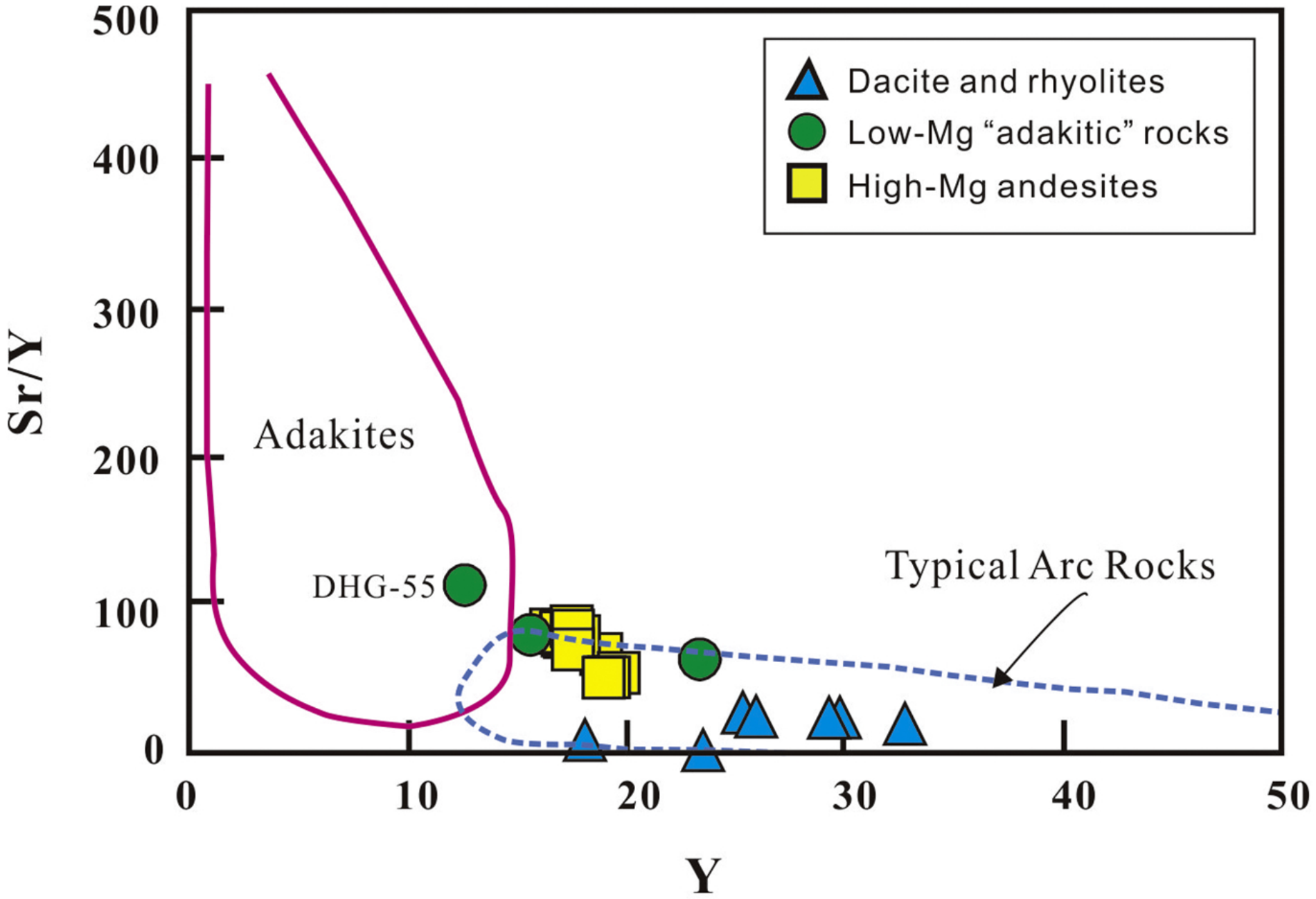
Dacite and rhyolites
Low-Mg "adakitic" rocks
High-Mg andesites
Adakites
DHG-55
Typical Arc Rocks
Sr/Y
Y
500
400
300
200
100
0
0
10
20
30
40
50

Figure 11

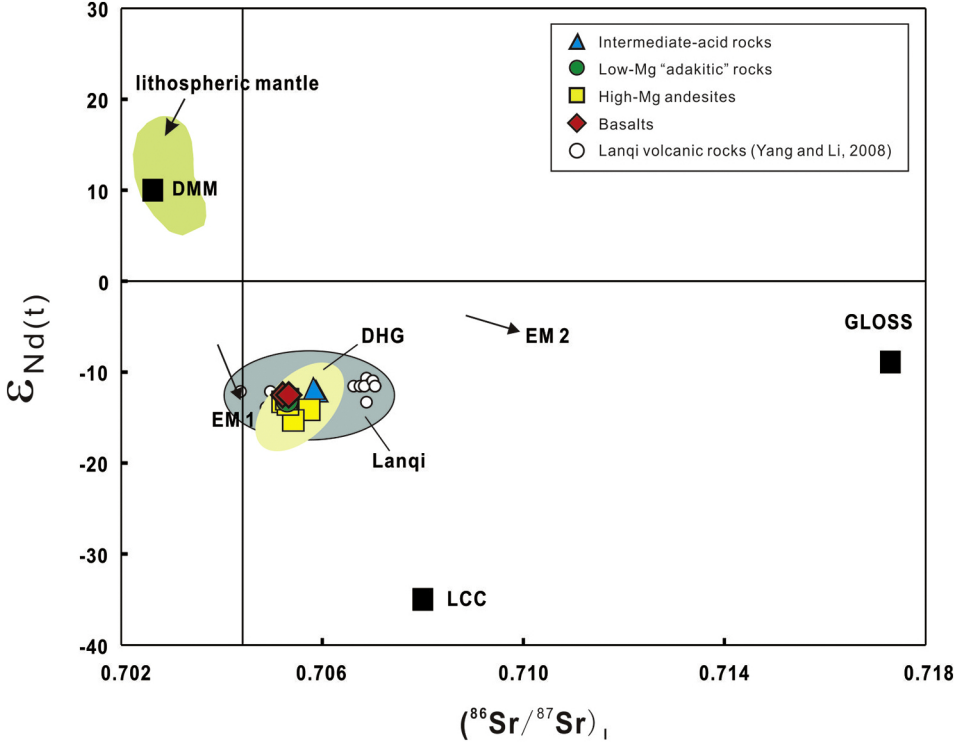
Intermediate-acid rocks
Low-Mg "adakitic" rocks
High-Mg andesites
Basalts
Lanqi volcanic rocks (Yang and Li, 2008)
lithospheric mantle
DMM
DHG
EM 2
GLOSS
EM 1
Lanqi
LCC
30
20
10
0
-10
-20
-30
-40
0.702
0.706
0.710
0.714
0.718
$\varepsilon_{Nd(t)}$
$(^{86}Sr/^{87}Sr)_i$

Figure 12

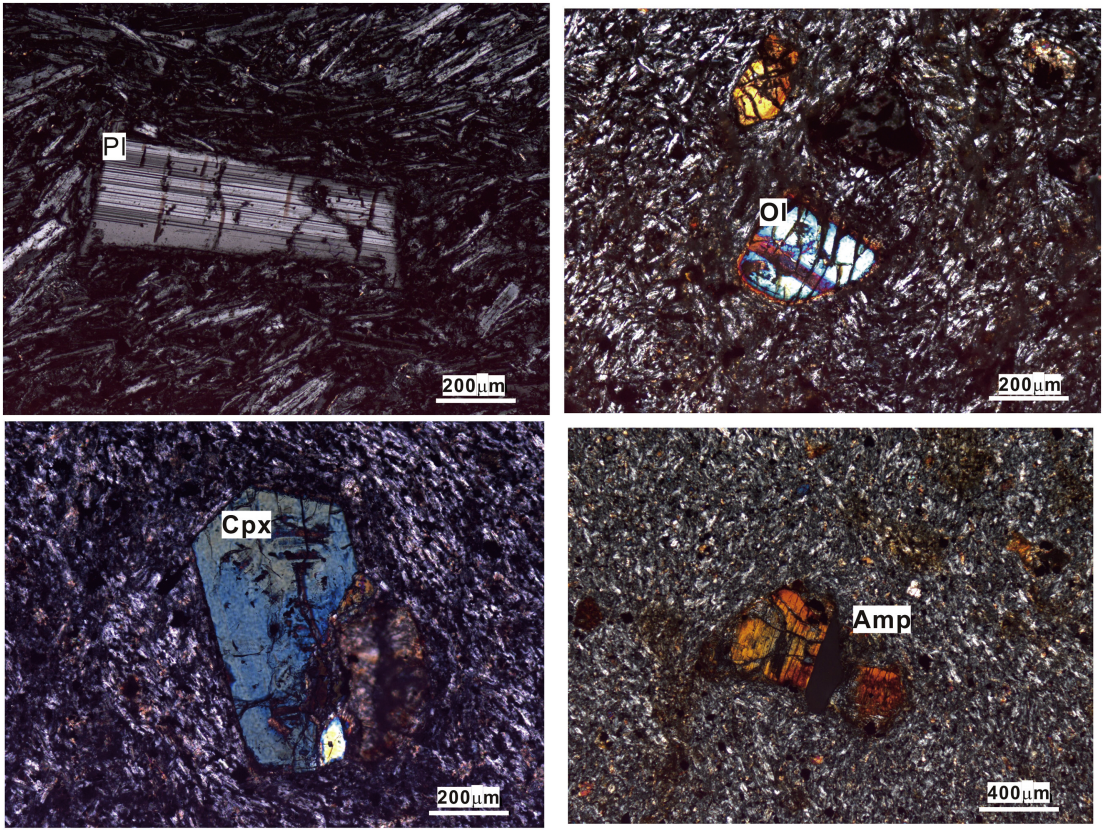

Figure 13

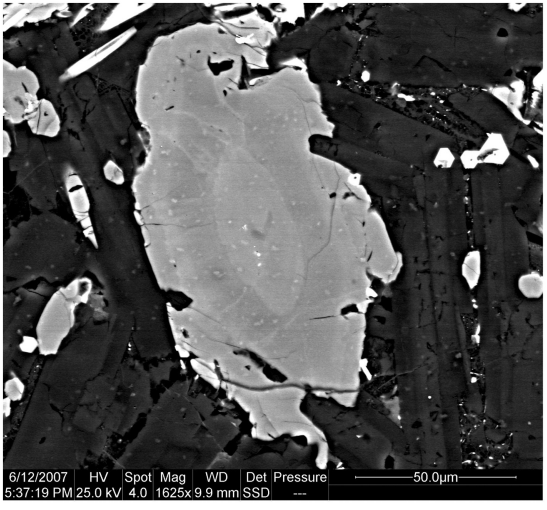
6/12/2007 HV Spot Mag WD Det Pressure
5:37:19 PM 25.0 kV 4.0 1625x 9.9 mm SSD ---
50.0µm

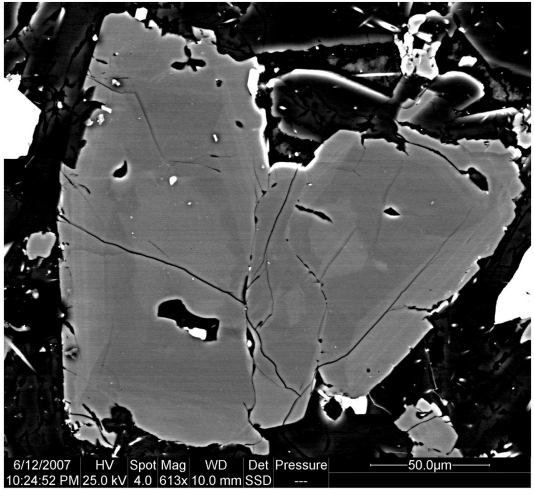
6/12/2007 HV Spot Mag WD Det Pressure
10:24:52 PM 25.0 kV 4.0 613x 10.0 mm SSD ---
50.0µm

Figure 14